To cite this version :

Enhancement of a dynamic vibration absorber by means of an electromagnetic shunt

Michel Auleley[1,3], Olivier Thomas[1] , Christophe Giraud-Audine[2] and Hervé Mahé[3]

Abstract

In this study, we address the reduction of structural vibrations by means of an electromagnetic shunt damper (EMSD) combined with a mechanical dynamic vibration absorber (DVA). Two architectures, that differs in the placement of the EMSD with respect to the DVA, are tested, showing that one of them enhances the vibration control. In parallel, three shunt architecture are tested: a resistive shunt, a resonant conservative shunt and a resonant dissipative shunt. Optimal values of the EMSD and DVA parameters are obtained; then, the performances of all architecture, according to relevant criteria, are estimated and compared to a single DVA or a single EMSD. The case of a conservative DVA, that creates an anti-resonance, is particularly targeted. It is shown that the performances rely on two free parameters only: the mass ratio for the DVA and the electromagnetic coupling factor for the EMSD, thus giving generic abacuses that can be applied to any practical cases. Finally, experiments are proposed and a good agreement with the theoretical results is obtained, thus validating them.

1. Introduction

Vibrations of mechanical systems and structures can be the cause of material fatigue, preliminary failure and unwanted noise. To reduce them, passive mechanical dampers are widely used (Connor and Laflamme, 2014). They consist in attaching to the host structure one or several simple mechanical one degree of freedom systems whose purpose is to counteract the oscillations and to dissipate energy as heat. The most well known principles are the Lanchester damper (Lanchester, 1914; Snowdon, 1968), composed of an inertia and a dashpot (Figure 1(d)) and the dynamic vibration absorber (DVA) (Frahm, 1911; Hartog, 1956), composed, in the conservative case, of an inertia and a spring (Figure 1(e)), or, in the general case, with a dashpot in addition (Figure 1(f)). If those mechanical dampers are used in many applications, their performances are linked to the value of the added mass: the more inertia is added to the host structure, the higher the damping performances are. This article explores the idea of coupling those mechanical dampers to an electromagnetic (EM) shunt damper, to enhance the

performances, or to achieve the same performances with a reduced added mass.

Since the early 90', electromechanical analogs of the mechanical dampers have been proposed, giving birth to the so-called electromechanical shunt dampers. In the pioneering works (Forward, 1979; Hagood and Von Flotow, 1991), a piezoelectric transduction is proposed, for which piezoelectric transducers glued on the host structure are shunted by a passive well-chosen impedance (see, among others (Thomas et al., 2012)). More recently (Behrens et al., 2003), the same idea has

[1]Arts et Metiers Institute of Technology, LISPEN, HESAM Université, Lille, France
[2]Arts et Metiers Institute of Technology, Univ. Lille, Centrale Lille, HEI, HESAM Université, Laboratoire d'Électrotechnique et d'Électronique de Puissance, Lille, France
[3]Valeo Transmissions, Centre d'Étude des Produits Nouveaux, Espace Industriel Nord, Amiens Cedex 1, France

Corresponding author:
Olivier Thomas, Arts et Metiers Institute of Technology, LISPEN, HESAM Université, 8 bd. Louis XIV, F-59000 Lille, France.
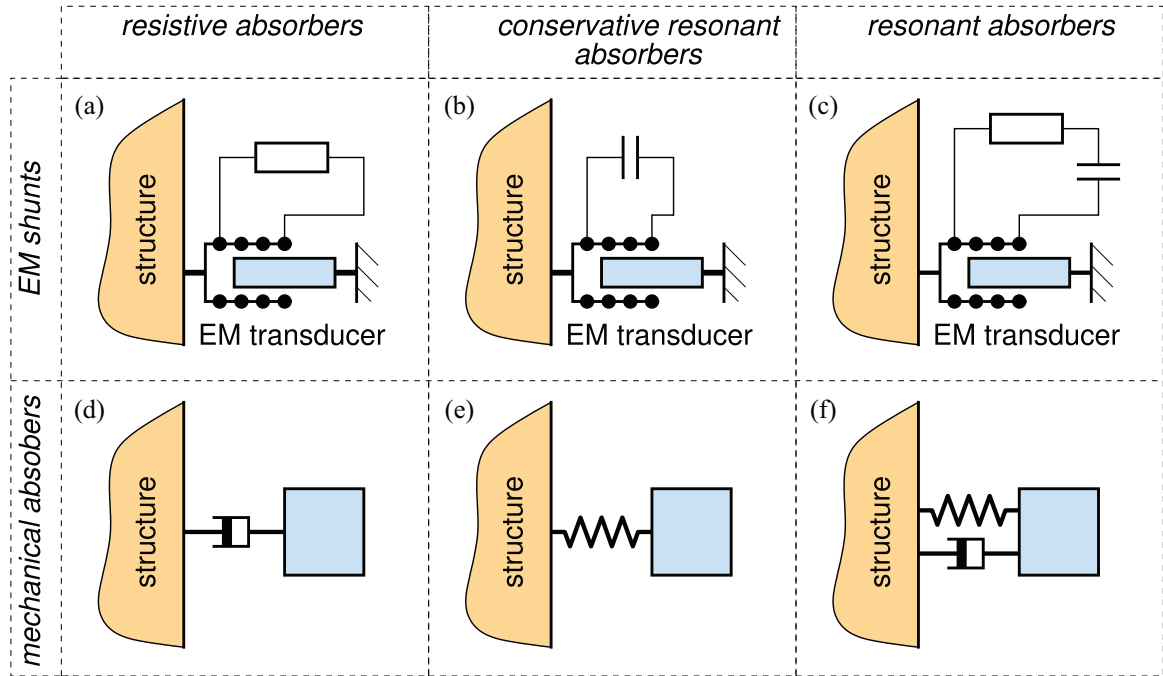Email: olivier.thomas@ensam.eu

Figure 1. Classical dampers: electromechanical (EM) shunts (first row) and mechanical dampers (second row). The symbols are described in the text and the European standards are used for resistors.

been proposed with an electromagnetic transducer shunted to a given electrical impedance, to obtain an electromagnetic shunt damper (EMSD). Because the coil acts as an inductance (equivalent to a mechanical inertia), one obtains a resistive shunt if the impedance is a pure resistor (R-shunt, Figure 1(a), analog of the Lanchester damper), a conservative resonant shunt if the impedance is a capacitor (C-shunt, Figure 1(b), analog of the conservative DVA) or a resonant shunt if a resistor is added (RC-shunt, Figure 1(c), analog of the DVA). Since the initial paper (Behrens et al., 2003), EMSD has been considered in various works, for vibration reduction or energy harvesting. The interested reader can refer to the review (Yan et al., 2017) for an exhaustive approach, whereas only a few major works are considered in the following. EM resonant shunts have been compared to a mechanical DVA in (Zhu et al., 2013) and optimum tuning parameters have been obtained in (Ao and Reynolds, 2019, 2020; Inoue et al., 2008; Tang et al., 2016; Zhou et al., 2019). Those works have been extended to multimode control (Cheng and Oh, 2009) and to adaptive tuning (McDaid and Mace, 2013; Niederberger et al., 2006). In parallel, resistive EM shunts have been considered as so-called passive EM dampers (Graves et al., 2000; Palomera-Arias et al., 2008; Zhu et al., 2012) or with negative impedances (Stabile et al., 2017; Yan et al., 2014). EM transducers have also been coupled to a mechanical DVA for semi-active control (Chung et al., 2013) or for energy harvesting (Takeya et al., 2016; Zuo and Cui, 2013). Tuned inertial dampers, associated to an

artificial increase of the mass ratio of a mechanical DVA using a rotational inertia (Krenk and Høgsberg, 2016), have also been coupled to an EM tranducer in (Asai et al., 2017; Nakamura et al., 2014). Finally, EM transducers can also be used with eddy current effects to obtain an equivalent viscous damping, directly on a structure (Sodano et al., 2005; Zuo et al., 2011) or to tune the dashpot of a mechanical DVA (Bae et al., 2012; Bourquin et al., 2014).

In the EMSD, an electromagnetic transducer has to be used to convert mechanical energy into electrical energy. A voice coil actuator (VCA) is often used, for which the energy transfer is obtained by means of a magnetic interaction between a coil and a permanent magnet (or an electromagnet) in relative motion. This phenomenon has a fundamental reversibility like piezoelectricity. The advantage of an electromagnetic transducer, in comparison to a piezoelectric transducer, is the possibility to oversize it in order to increase the electromechanical coupling. Indeed, in the case of a piezoelectric transducer, the electromechanical coupling mainly depends on the piezoelectric material properties, which limits it. On the contrary, the coupling factor for electromagnetic transducers is an increasing function of its mass, as shown in (Elliott and Zilletti, 2014). The other difference between piezoelectric and electromagnetic shunts is the placement of the transducer on the host structure. Since piezoelectric materials are sensible to mechanical strains, they are suitable for deformable structures and they have to be located at the maxima of strains. On the contrary, electromagnetic transducers
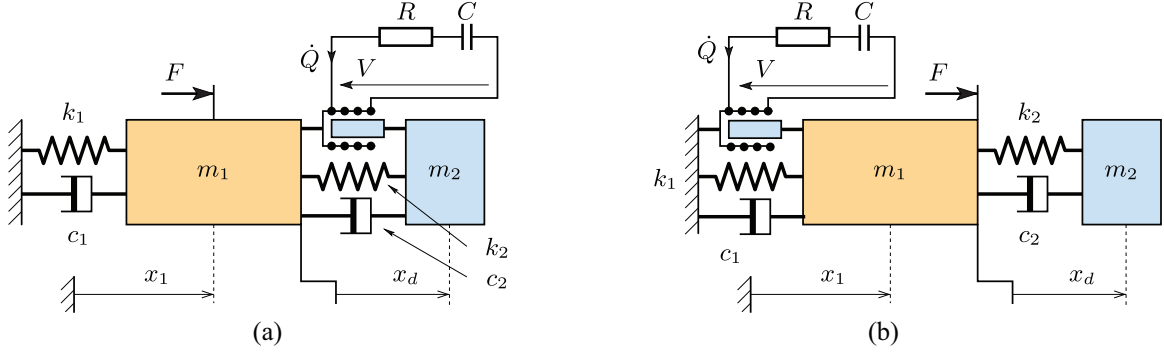
Figure 2. Scheme of the proposed architectures to couple a mechanical DVA and an electromechanical damper.

are sensible to a relative motion between the coil and the magnet and have to be located on maxima of displacement of the host system. They are thus naturally suitable for rigid solid assemblies as well as elastic structures. Finally, a major difference between piezoelectric and electromagnetic transducers is the non negligible internal resistance of the latter, which is sometimes too high and which requires the use of negative resistance to optimise the shunts.

In this paper, we investigate the addition of an electromagnetic shunt damper (EMSD) to a mechanical damper to increase the performances of vibration reduction. The study is limited to forced vibrations in the vicinity of a given resonance of the host system, which is thus modelled for simplicity as a single degree of freedom mechanical oscillator. Naturally, we have two solutions to place the EMSD, as shown in Figure 2. In architecture 1 (Figure 2(a)), the EMSD is placed within the DVA, in parallel of its stiffness ; in architecture 2 (Figure 2(a)), the EMSD is placed between the primary system and the frame. In practice, those two architectures lead to different designs since for architecture 1, one would modify the design of the DVA to include the EM transducer, whereas in architecture 2, the DVA design is not changed and the transducer has to be included in the primary structure. We mainly focus on a conservative or nearly conservative mechanical damper, because of its particular property of creating an anti-resonance an thus of cancelling the vibrations of the primary system at this particular frequency. By analysing the frequency responses, we obtain that architecture 2 shows better performances with a nearly conservative mechanical damper. Then, focusing on architecture 2, both conservative and dissipative cases for the EMSD are considered. It is shown that the effect of the EMSD is to mitigate the negative effect of the two side resonances, by increasing their distance to the anti-resonance and by decreasing their sharpness. In each case, we determine the optimal values of the parameters of the two dampers (the mechanical and the EMSD) to maximise the vibration reduction. In addition, some generic charts are

proposed to characterise the vibration damping performances as a function of the two free parameters of the system: the mass ratio of the mechanical damper and the electromechanical coupling factor of the EMSD.

The paper is organised as follows: in section 2, the main properties of the basic mechanical and EM dampers are introduced, in term of frequency response, tuning and performances. Then, in section 3 and 4, the theoretical behaviour of the two coupled architectures is addressed in details, focusing on exhibiting closed form solutions for their tuning, to improve the vibration reduction. Finally, some validation experiments are proposed in section 5.

2. Mechanical dampers and electromagnetic shunts

In this section, we consider separately the two families of dampers: on the one hand the mechanical dampers (Figure 1(d)–(f)) and on the other hand the electromagnetic shunts (Figure 1(a)–(c)). The purpose is to briefly recall already known results about the tuning of the dampers, to extend them to derive the performance of those dampers in forced vibrations and to compare them. The free parameters that governs the performances (the mass ratio and the electromechanical coupling factor) are introduced and characterised as figure of merit of the dampers. This section is a preliminary to sections 3 and 4, in which the coupling of those two elementary dampers will be studied. Moreover, the proposed comparison of all the six dampers of Figure 1, in term of figure of merit, attenuation performance and design charts, is original to the knowledge of the authors.

2.1. Governing equations for the mechanical dampers

We first consider the system of Figure 3(a), composed of a primary host system of mass m_1, stiffness k_1 and viscous damping constant c_1 coupled to a mechanical damper of mass m_2, stiffness k_2 and viscous damping
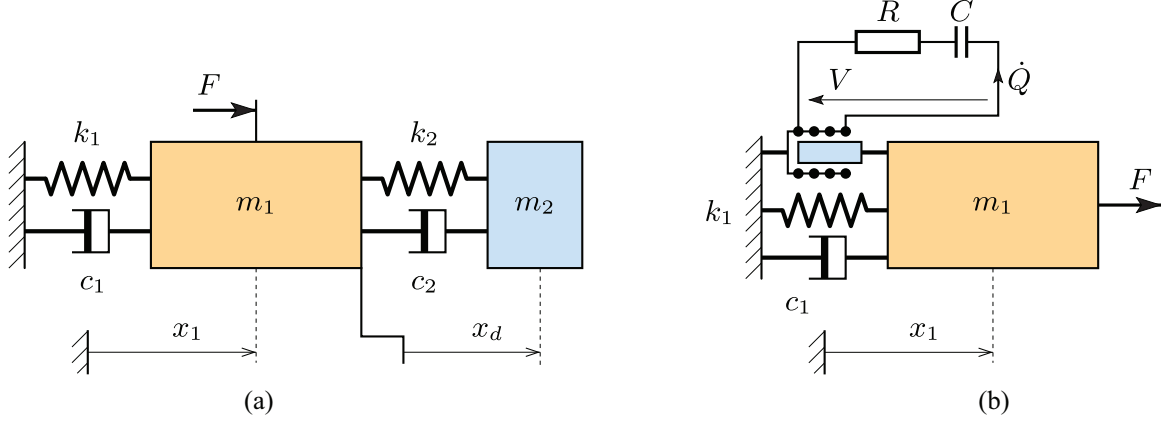
Figure 3. Standard passive dampers coupled to a one degree of freedom host structure: (a) a DVA; (b) a RC-shunt.

constant c_2. The displacement of m_1 is denoted by $x_1(t)$ and the relative displacement of m_2 with respect to m_1 is denoted by $x_d(t)$ as a function of time t. Those displacement being measured with respect to the equilibrium state of the system, they verify the following equations:

$$(m_1 + m_2)\ddot{x}_1 + m_2\ddot{x}_d + c_1\dot{x}_1 + k_1 x_1 = F, \qquad (1a)$$

$$m_2\ddot{x}_d + m_2\ddot{x}_1 + c_2\dot{x}_d + k_2 x_d = 0. \qquad (1b)$$

Depending of the type of damper considered (Lanchester, conservative DVA (CDVA) or DVA, Figure 1(c)–(e)), the parameters c_2 or k_2 can be set to zero. By dividing the above equations by respectively m_1 and m_2, they are rewritten as:

$$(1 + \mu)\ddot{x}_1 + \mu\ddot{x}_d + 2\xi_1\omega_1\dot{x}_1 + \omega_1^2 x_1 = F/m_1, \qquad (2a)$$

$$\ddot{x}_d + \ddot{x}_1 + \lambda\dot{x}_d = 0, \qquad \text{Lanchester} \qquad (2b)$$

$$\ddot{x}_d + \ddot{x}_1 + \omega_2^2 x_d = 0, \qquad \text{CDVA} \qquad (2c)$$

$$\ddot{x}_d + \ddot{x}_1 + 2\xi_2\omega_2\dot{x}_d + \omega_2^2 x_d = 0. \quad \text{DVA} \qquad (2d)$$

The three last equations are relative to a given type of mechanical damper, as mentioned. The introduced parameters are:

$$\mu = \frac{m_2}{m_1}, \quad \omega_1 = \sqrt{\frac{k_1}{m_1}}, \quad \omega_2 = \sqrt{\frac{k_2}{m_2}}, \quad \xi_1 = \frac{c_1}{2\sqrt{k_1 m_1}},$$

$$\xi_2 = \frac{c_2}{2\sqrt{k_2 m_2}}, \quad \lambda = \frac{c_2}{m_2}. \qquad (3)$$

where μ is the mechanical damper mass ratio, the ratio between the added mass m_2 to the mass of the primary system m_1. Moreover, ω_1, ξ_1 are respectively the natural frequency and the damping ratio of the primary system; ω_2, ξ_2 are respectively the natural frequency and the damping ratio of the DVA and λ is the decay rate of the Lanchester damper (homogeneous to the inverse of a time).

It is convenient to introduce the natural frequency $\omega_{1,\infty}$ of the primary system in the limit case of a damper mass m_2 blocked on m_1 (obtained if $c_2 \to +\infty$ or $k_2 \to +\infty$), that writes:

$$\omega_{1,\infty} = \sqrt{\frac{k_1}{m_1 + m_2}}. \qquad (4)$$

One can then easily show that the mass ratio can be written as follows:

$$\mu = \frac{\omega_1^2 - \omega_{1,\infty}^2}{\omega_{1,\infty}^2}, \qquad (5)$$

which shows that it depends on the limit natural frequencies of the primary system only.

2.2. Governing equations for the EMSD

We now consider the EMSD of Figure 3(b) for which the primary system is coupled to an electronic circuit (a resistor R and a capacitance C) through an electromagnetic transducer. The governing equations are:

$$m_1\ddot{x}_1 + c_1\dot{x}_1 + k_1 x_1 + \phi\dot{Q} = F, \qquad (6a)$$

$$L\ddot{Q} + V - \phi\dot{x}_1 = 0. \qquad (6b)$$

Equation (6a) is the second Newton's law applied to mass m_1, subjected to the action of the EM transducer. The latter produces a force $\phi\dot{Q}$ proportional to the current intensity in the electrical circuit, where $Q(t)$ is the electric charge in the EM transducer. Equation (6b) is the Kirchhoff's law applied to the electrical circuit, in which the EM transducer is equivalent to an inductor of constant L and an electromotive force $\phi\dot{x}_1$ proportional to the relative velocity of the coil and the magnet in the transducer. Here, we consider a perfect EM transducer, with no internal resistance, the whole resistance of the circuit being modelled by the resistance of the shunt R. Since in practice (see section 5) EM

transducer have an internal resistance, in the model and without loss of generality, it is considered as a part of R. Parameter ϕ (of units N/A or V/(m/s)) is the force factor of the EM transducer. For a simple moving coil actuator, with a coil of N turns of length l coupled to a permanent magnet creating a magnetic flux B, the force factor is $\phi = BNl$.

To obtain generic equations, it is convenient to scale the electrical quantities to obtain equivalent mechanical variables. $Q(t)$ and $V(t)$ are replaced by:

$$\bar{Q} = \sqrt{\frac{L}{m_1}}Q, \qquad \bar{V} = \frac{1}{\sqrt{m_1 L}}V, \qquad (7)$$

where $\bar{Q}$ is homogeneous to a displacement and $\bar{V}$ to a force per unit mass. Equations (6(a,b)) then become:

$$\ddot{x}_1 + 2\xi_1\omega_1\dot{x}_1 + \omega_1^2 x_1 + \kappa\omega_1\dot{\bar{Q}} = \frac{F}{m_1}, \qquad (8a)$$

$$\ddot{\bar{Q}} + \bar{V} - \kappa\omega_1\dot{x}_1 = 0, \qquad (8b)$$

where the dimensionless electromechanical coupling factor (EMCF) κ has been introduced.

$$\kappa = \frac{\phi}{\omega_1\sqrt{m_1 L}}. \qquad (9)$$

This last parameter can also be obtained as a function of the natural frequencies of the primary system with the electric circuit in open circuit (OC, $\dot{Q} = 0$) $\omega_{1,oc} = \omega_1$ and in short circuit (SC, $V = 0$) $\omega_{1,sc}$. In SC, imposing $V = 0$ in equation (6b) implies after time integration :

$$\dot{Q} = \frac{\phi}{L}x + i_0, \qquad (10)$$

with i_0 an integration constant. If there is no displacement (i.e. $x_1 = 0$), there is no electric current induced (i.e. $\dot{Q} = 0$), so this integration constant is zero (i.e. $i_0 = 0$). Using equation (10) into equation (6a), one obtains:

$$\ddot{x}_1 + 2\xi_1\omega_1\dot{x} + \omega_{1,sc}^2 x = \frac{F}{m}, \qquad (11)$$

with:

$$\omega_{1,sc} = \omega_1\sqrt{1 + \kappa^2}. \qquad (12)$$

which finally shows that the EMCF can be written:

$$\kappa = \sqrt{\frac{\omega_{1,sc}^2 - \omega_{1,oc}^2}{\omega_{1,oc}^2}}. \qquad (13)$$

The above formula is analogous to the one that defines the effective EMCF in the case of a piezoelectric transducer (ANSI/IEEE Std 176-1987, 1988; Thomas et al., 2009), except that in the present case, the roles of the

OC and SC natural frequencies are exchanged. Moreover, it shares a clear similarity with equation (5) in the case of the mechanical damper, with μ playing the role of κ^2.

Considering the RC electrical circuit, $V(t) = R\dot{Q} + Q/C$, and the three types of shunts (Figure 1(a)–(c)), equation (8b) is replaced by:

$$\ddot{\bar{Q}} + \lambda_e\dot{\bar{Q}} - \kappa\omega_1\dot{x}_1 = 0, \qquad \text{R} - \text{shunt} \qquad (14a)$$

$$\ddot{\bar{Q}} + \omega_e^2\bar{Q} - \kappa\omega_1\dot{x}_1 = 0, \qquad \text{C} - \text{shunt} \qquad (14b)$$

$$\ddot{\bar{Q}} + 2\xi_e\omega_e\dot{\bar{Q}} + \omega_e^2\bar{Q} - \kappa\omega_1\dot{x}_1 = 0, \qquad \text{RC} - \text{shunt} \qquad (14c)$$

where each equation is relative to a given type of shunt, as mentioned. The introduced parameters are the decay rate λ_e of the electrical circuit in the resistive case, its damping ratio ξ_e and natural frequency ω_e in the resonant case:

$$\lambda_e = \frac{R}{L}, \qquad \omega_e = \frac{1}{\sqrt{LC}}, \qquad \xi_e = \frac{R}{2}\sqrt{\frac{C}{L}}. \qquad (15)$$

2.3. Tuning, performances and comparison

Both family of dampers (mechanical and EMSD) have the same behaviour of coupling the primary resonant system to either a resistive or a resonant secondary system (compare equations (2a–d) for the mechanical dampers and equations (8a)–(14a–c) for the EMSD). Their optimisation, that is, the choice of optimal values for the parameters of the dampers to maximise the vibration reduction of the primary system has been already published in many texts and only the results are recalled here. First of all, the choice of the optimisation criteria has to be specified and the dissipative cases (resistive or resonant dampers, Figure 1(a), (c), (d) and (f)) are different than the conservative case (conservative resonant dampers, Figure 1(b) and (e)).

We consider periodic oscillations of the system under harmonic forcing $F(t) = F_0 \cos\Omega t$, at frequency Ω. Fourier transforms of the time functions are denoted by a hat (for instance, $\hat{x}_1(\Omega)$ is the Fourier transform of $x_1(t)$).

2.3.1. Dissipative cases.
In the dissipative cases, we choose to optimise the vibration damping by reducing as much as possible the maximal amplitude of the primary system $|\hat{x}_1(\Omega)|$ as a function of the excitation frequency Ω, a so called H_∞ optimisation. In the case of the resistive dampers, Figure 4 shows the frequency response of x_1, defined by equations (2a,b) and (8a)–(14a) in the frequency domain, for several values of the absorber viscous damping parameters λ and λ_e. It is found that the curves have always the shape of a resonance and that the resonance point follows a particular

Figure 4. Frequency response $|\hat{x}_1|/|\hat{x}_1(\Omega = 0)|$ of the system with resistive dampers, for $\xi_1 = 0.01$, $\mu = \kappa^2 = 0.05$. The type of damper is specified close to the corresponding curve.
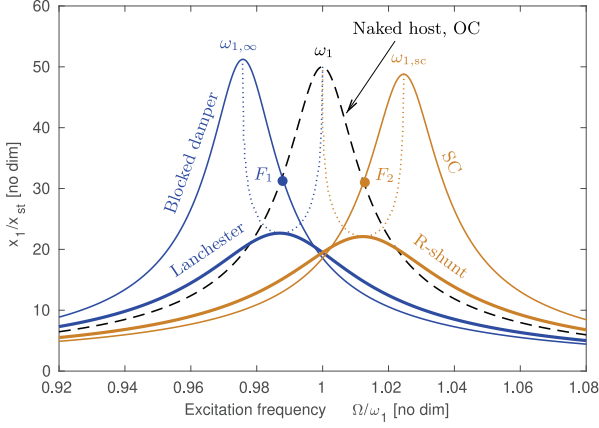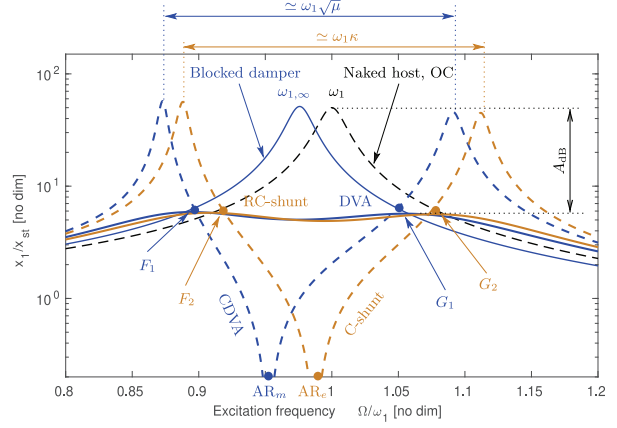

Figure 5. Frequency response $|\hat{x}_1|/|\hat{x}_1(\Omega = 0)|$ of the system with resonant dampers, for $\xi_1 = 0.01$, $\mu = \kappa^2 = 0.05$, $\omega_2 = \omega_{2,\text{opt}}$, $\omega_e = \omega_{e,\text{opt}}$. The type of damper is specified close to the corresponding curve.

curve in the $(|\hat{x}_1|, \Omega)$ plane, shown in dotted line in Figure 4. It has been computed numerically. Its minimum corresponds to the optimised response. It is found for particular values λ_{opt} and $\lambda_{e,\text{opt}}$ of λ and λ_e, obtained by the fixed point method (Snowdon, 1968; Thomas et al., 2012; Vakilinejad et al., 2019). Briefly, if the damping of the primary system is neglected ($\xi_1 = 0$), it is found that all the frequency response curves crosses each other at a single 'fixed' point (labelled F_1 for the Lanchester damper and F_2 for the R-shunt in Figure 4). The coordinates of this point are known in closed form and enable to find the optimised response whose maxima lie exactly at this fixed point. If $\xi_1 \neq 0$, it is found that this optimisation gives excellent results even if the resonance point of the optimal response is slightly below the fixed points F_1 and F_2 (the case shown in Figure 4) (see e.g. Thomas et al., 2012; Vakilinejad et al. 2019). The optimal values λ_{opt} and $\lambda_{e,\text{opt}}$ are given in Table 1.

Figure 4 also shows the system's frequency response in its three limit cases: (i) the host structure without the mechanical absorber ('naked'), equivalent to the case with the EM transducer in open circuit (OC). The

response has a resonance close to $\Omega = \omega_1$; (ii) the system with the absorber mass m_2 glued to the primary mass ('blocked damper' case); it resonates at $\Omega \simeq \omega_{1,\infty}$, which is lower than ω_1 (see equation (4)); (iii) the system with the EM transducer in short circuit (SC), that resonates at $\Omega \simeq \omega_{1,\text{sc}}$, which is greater than ω_1 (see equation (12)).

In the case of resonant dampers, Figure 5 shows the frequency response of x_1, defined by equations (2a,d) and (8a)–(14c) in the frequency domain, for several values of the absorber viscous damping parameters ξ_2 and ξ_e. When $\xi_2 = 0$ or $\xi_e = 0$, the conservative dampers cases are obtained and two resonances appear instead of one in the naked/OC case. When ξ_2 or ξ_e are varied, the resonance points of the system moves in the $(|\hat{x}_1|, \Omega)$ plane and optimal cases are obtained. They can be estimated by the fixed point method, analogous to the resistive case, for which two fixed point are obtained (labelled (F_1, G_1) for the DVA and (F_2, G_2) for the RC-shunt in Figure 5) (Connor and Laflamme, 2014; Hartog, 1956; Inoue et al., 2008; Krenk, 2005; Liu and

Table 1. Optimum parameters and characteristics of mechanical, electromagnetic shunts and coupled dampers of architecture 2.

Damper	Mechanical Figure 3(a)	EM shunt Figure 3(b)	CDVA + EM shunt Figure 2(b)
Resonant conservative	$\omega_2^{\text{opt}} = \omega_1$ $\Delta\omega \simeq \omega_1\sqrt{\mu}$	$\omega_e^{\text{opt}} = \omega_1$ $\Delta\omega \simeq \omega_1\kappa$	$\omega_e^{\text{opt}} = \omega_2^{\text{opt}} = \omega_1$ $\Delta\omega \simeq \omega_1\sqrt{\mu + \kappa^2}$
Resitive	$\lambda^{\text{opt}} = \omega_1\sqrt{\dfrac{2}{2+\mu}}$ $\omega_{1,\infty} = \dfrac{\omega_1}{\sqrt{1+\mu}}$	$\lambda_e^{\text{opt}} = \omega_1\sqrt{\dfrac{2+\kappa^2}{2}}$ $\omega_{1,\text{sc}} = \omega_1\sqrt{1+\kappa^2}$	$\lambda^{\text{opt}} = \omega_1\sqrt{1 + \dfrac{\mu}{2} + \dfrac{\kappa^2}{4}}$
Resonant dissipative	$\omega_2^{\text{opt}} = \dfrac{\omega_1}{1+\mu}$ $\xi_2^{\text{opt}} = \sqrt{\dfrac{3\mu}{8(1+\mu)}}$	$\omega_e^{\text{opt}} = \omega_1\sqrt{\dfrac{2-\kappa^2}{2}}$ $\xi_e^{\text{opt}} = \sqrt{\dfrac{3\kappa^2}{4(2-\kappa^2)}}$	$\omega_e^{\text{opt}} = \omega_2^{\text{opt}} = \omega_1\sqrt{\dfrac{2-\kappa^2}{2(1+\mu)}}$ No simple expression

When a '=' sign is used, the expression is exact, whereas when ';' is used, it means that it is approximated, with $\mu \ll 1$ and/or $\kappa^2 \ll 1$.

Liu, 2005; Thomas et al., 2012; Zhou et al., 2019). The optimal DVA or RC-shunt curves have the shape of a smooth curve for which the two resonances have almost disappeared and are close to the fixed points. The optimal values of (ω_2, ξ_2) for the DVA and (ω_e, ξ_e) for the RC-shunt are given in Table 1.

To measure the performance of the damping, we define the following performance indicator referred to as the attenuation (in decibels):

$$A_{dB} = 20 \log \frac{X_{0,\max}}{X_{opt,\max}}, \quad (16)$$

with $X_{0,\max}$ the displacement amplitude of the primary system without absorber at its resonance $\omega_{1,r} = \omega_1 \sqrt{1 - 2\xi_1^2}$,

$$X_{0,\max} = \frac{F_0}{m_1 \omega_1^2} \frac{1}{2\xi \sqrt{1 - \xi^2}}, \quad (17)$$

and $X_{opt,\max}$ the same with the primary system connected to the optimally tuned absorber. Following the same ideas as in (Berardengo et al., 2016; Ducarne et al., 2010; Thomas et al., 2012; Vakilinejad et al., 2019) for piezoelectric shunts and Lanchester dampers, a good estimation of A_{dB} is obtained by approximating $X_{opt,\max}$ by the amplitude of the damped frequency response (with $\xi_1 \neq 0$) at the frequency of the fixed points F_1, F_2, G_1, G_2 for optimal values of the parameters λ, ω_2, ξ_2, λ_e, ω_e and ξ_e of Table 1. Whereas analytical expressions for A_{dB} could be exhibited, we simply compute it numerically in the present text, using the values of the fixed point frequencies given in Appendix 1, for the four dampers (Lanchester, DVA, R-shunt and RC-shunt).

A major result is that A_{dB} depends on only two parameters: the primary damping ratio ξ_1 and the coupling factor (μ for the mechanical dampers and κ for the EMSDs). Figure 6 shows A_{dB} as a function of these two parameters. First, on can remark that for a given ξ_1, A_{dB} is an increasing function of the coupling factor μ or κ. It thus demonstrate that μ (for the mechanical dampers) and κ (for the EMSDs) are the
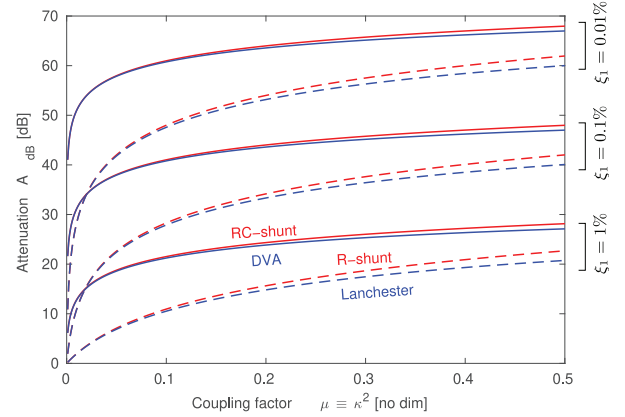

Figure 6. Attenuation A_{dB} of the displacement x_1 as a function of the coupling factor(μ for the mechanical dampers; κ^2 for the EMSD) for the dissipative dampers, for several values of the primary system damping ratio ξ_1, as specified. The blue curves correspond to the mechanical dampers ('—': DVA; '- -': Lanchester) and the red curves to the EM dampers ('—': RC-shunt; '- -': R-shunt).

damper and EMSD when $\kappa^2 = \mu$, with a slight advantage for the EMSD. This further demonstrates the equivalence between the mechanical dampers and the EMSDs, as shown in (Zhu et al., 2013) in the case of the resonant dampers (DVA and RC-shunt). Also, the weaker ξ_1 is, the larger the attenuation A_{dB} is. In addition, one observes that the resonant damper is more efficient than the resistive one for a same ξ_1.

2.3.2. Conservative cases.
In the case of conservative resonant dampers (equations (2a,c) and (8a)–(14b)), the situation is different since it is not possible to attenuate a given resonance peak thanks to an addition of viscous damping. The principle is to create an anti-resonance for x_1. Namely, a particular excitation frequency ω_{ar} exists for which the amplitude of the host structure is zero: $|\hat{x}_1(\omega_{ar})| = 0$. This is a strict zero even if $\xi_1 \neq 0$ and this anti-resonance frequency is exactly the natural frequency of the damper: $\omega_{ar} = \omega_2$ for the CDVA and $\omega_{ar} = \omega_e$ for the RC-shunt, as shown in Figure 5 with labels AR_m and AR_e. To prove this result, one has just to write $\hat{x}_1(\Omega)$ from equations (2a,c) and (8a)–(14b):

$$\hat{x}_1(\Omega) = \frac{F_0}{m_1} \frac{-\Omega^2 + \omega_2^2}{\Omega^4 - \left[\omega_1^2 + (1 + \mu)\omega_2^2\right]\Omega^2 + \omega_1^2\omega_2^2 + 2j\xi_1\omega_1\Omega(\omega_2^2 - \Omega^2)}, \quad \text{(CDVA)} \quad (18a)$$

$$\hat{x}_1(\Omega) = \frac{F_0}{m_1} \frac{-\Omega^2 + \omega_e^2}{\Omega^4 - \left[(1 + \kappa^2)\omega_1^2 + \omega_2^2\right]\Omega^2 + \omega_1^2\omega_e^2 + 2j\xi_1\omega_1\Omega(\omega_e^2 - \Omega^2)}, \quad \text{(C − shunt)} \quad (18b)$$

sole optimisation parameters that guarantee the damping performances. Furthermore, similar damping performances are obtained between equivalent mechanical

where $j = \sqrt{-1}$ and for which the numerators vanish at $\Omega = \omega_{ar}$. The optimisation consists in tuning the damper in order to generate the anti-resonance at a frequency of interest. Here, we choose $\omega_{ar} = \omega_1$ ($\omega_2 = \omega_1$ for the CDVA and $\omega_e = \omega_1$ for the C-shunt) to

transform the resonance of the primary system into an anti-resonance.

However, as shown in Figure 5, two adjacent resonances appear on the sides of the anti-resonance, whose frequencies can be obtained with the poles of equations (18a,b). If ξ_1 is small, those resonance frequencies are close to the natural frequencies of the whole system, obtained with $\xi_1 = 0$:

$$\omega_{2\pm} = \omega_1 \sqrt{\frac{2 + \mu}{2} \pm \sqrt{\frac{4\mu + \mu^2}{4}}} \simeq \omega_1 \left(1 \pm \frac{\sqrt{\mu}}{2}\right), \text{(CDVA)} \quad (19a)$$

$$\omega_{e\pm} = \omega_1 \sqrt{\frac{2 + \kappa^2}{2} \pm \sqrt{\frac{4\kappa^2 + \kappa^4}{4}}} \simeq \omega_1 \left(1 \pm \frac{\kappa}{2}\right), \text{(C − shunt)} \quad (19b)$$

where the approximations in the above equations are valid for small μ and κ. One can observe that the resonance frequencies ratio $\omega_{2\pm}/\omega_1$ and $\omega_{e\pm}/\omega_1$ depend solely on the coupling factors μ and κ^2. Then, a performance indicator for those absorbers can be chosen as the frequency distance $\Delta\omega$ between the two resonance peaks, that can be approximated for small μ and κ by:

$$\Delta\omega \simeq \omega_1 \sqrt{\mu}, \text{(CDVA)} \quad \Delta\omega \simeq \omega_1 \kappa, \text{(C − shunt)} \quad (20)$$

summarised in Table 1. As a consequence, the same conclusions as in the dissipative case can be given here. First, the coupling factors μ and κ are the design parameters that guarantee the performances: the larger they are, the larger is the useful frequency band $\Delta\omega$ around the anti-resonance. Then, μ and κ^2 have an equivalent effect on the mechanical dampers and the EMSDs, respectively.

2.4. Analogies between dampers

All throughout the paper, we consider the dampers depicted in Figure 1 and combinations of them. To compare mechanical and electromechanical dampers, we use the Maxwell analogy (Maxwell, 1865) (also called impedance analogy (Busch-Vishniac, 1999)), in which an electric current is considered as the analog of a mechanical velocity and a voltage as the analog of a mechanical force. In this analogy, inductance and capacitance are analogous respectively to a mechanical mass and a compliance and electrical equations, which write as function of electric charges, are directly comparable to mechanical equations written in term of displacements. This point of view justifies the equivalence between the EM dampers and the mechanical dampers in Figure 1.

One can also choose the opposite convention, leading to the Firestone (or mobility) analogy, in which electrical current and voltage are analogous respectively to a force and a velocity (Firestone, 1933). In this case, inductance and capacitance are analogous respectively to a stiffness and a particular mechanical element called an inerter (Smith, 2002) and the EM dampers of the first row of Figure 1 are analogous to mechanical dampers built with inerters, springs and dashpots in series.

In the present study, we choose to gather the dampers in families in which they share similar dynamical behaviours. For instance, the DVA (Figure 1(f)) is equivalent to an inerter based absorber, as proved in (Krenk and Høgsberg, 2016), and also to other architectures in which the mechanical elements are in series rather than in parallel (Høgsberg, 2020). Those mechanical absorbers are also analogous to the resonant EM shunt damper of Figure 1(c), or the same shunt with C and R in parallel. There is also an analogy with a piezoelectric resonant shunt, with the circuit in series or in parallel (Caruso, 2001; Thomas et al., 2012). All those dampers, called here *resonant*, share similar response curve such as the one of Figure 5. With the same logic, the dampers of Figure 1(a) and (d) are called *resistive* and the ones of Figure 1(b) and (e)*resonant conservative* since no dissipative element (an electrical resistance or a dashpot) is used in the damper. One must notice that all those equivalence are not perfect: this justify the slight differences of behaviour noticed in Figure 6, between on the one hand the mechanical dampers (DVA and Lanchester) and on the other end the EM dampers (RC-shunt and R-shunt).

3. Coupled architecture 1: EMSD between the host structure and the mechanical damper

We consider in this section the first coupled DVA/EMSD architecture, shown in Figure 2(a), for which the EMSD is placed in parallel of the stiffness of the DVA. In the litterature, this kind of architecture has been considered for energy harvesting application, in which the EM transducer is used to convert the vibration energy of the DVA into electrical energy (Liu et al., 2016; Tang and Zuo, 2011; Zuo and Cui, 2013). Here, we restrict ourselves to the case of vibration reduction of the primary system. We also consider here only the case of purely conservative absorbers, that is, a CDVA and a C-shunt ($c_2 = 0$, $R = 0$) coupled to a dissipative primary system ($\xi_1 \neq 0$). The case of dissipative absorbers has been considered previously in (Barredo et al., 2018; Høgsberg, 2019), with respectively inerter based absorbers and piezoelectric shunts. Using the same approach as in section 2 for equations (2a–d), (8a,b), (14a–c), the governing equations of this system are:

$$(1 + \mu)\ddot{x}_1 + \mu\ddot{x}_d + 2\xi_1\omega_1\dot{x}_1 + \omega_1^2 x_1 = \frac{F}{m_1}, \quad (21a)$$
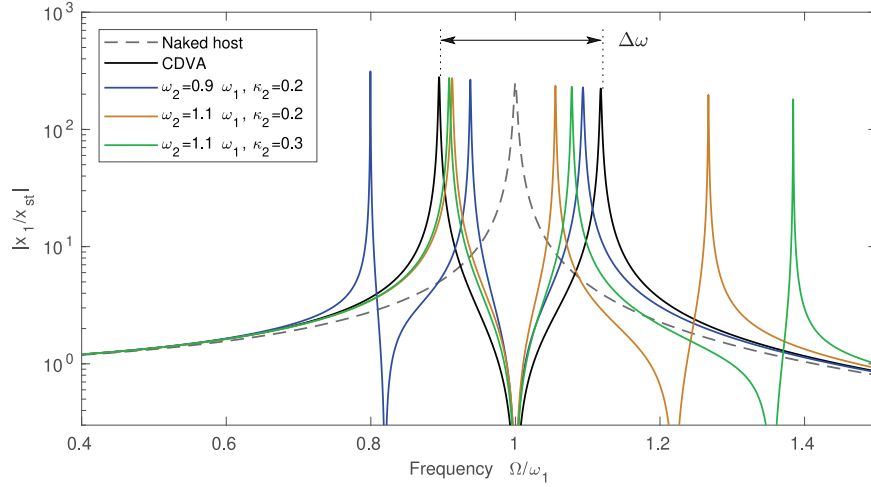
Figure 7. Frequency response $|\hat{x}_1|/|\hat{x}_1(\Omega = 0)|$ of the primary mass displacement for architecture 1, for some values of the DVA natural frequency ω_2 and the EM coupling factor κ_2, as specified in the legend. The electrical frequency ω_e is chosen according to equation (26) to enforce an anti-resonance at ω_1. The mass ratio is $\mu = 0.05$ and the damping ratio $\xi_1 = 0.002$.

$$\ddot{x}_d + \ddot{x}_1 + \omega_2^2 x_d + \kappa_2 \omega_2 \dot{\bar{Q}} = 0, \tag{21b}$$

$$\ddot{\bar{Q}} + \omega_e^2 \bar{Q} - \kappa_2 \omega_2 \dot{x}_d = 0, \tag{21c}$$

with $\bar{Q}$ the equivalent electrical charge, $\bar{V}$ the equivalent voltage and κ_2 the EMCF:

$$\bar{Q} = \sqrt{\frac{L}{m_2}} Q, \quad \bar{V} = \frac{1}{\sqrt{m_2 L}} V, \quad \kappa_2 = \frac{\phi}{\omega_2 \sqrt{m_2 L}}. \tag{22}$$

The frequency responses of this system are:

$$\hat{x}_1 = \frac{F_0}{m_1} \frac{\Omega^4 - \left[(1 + \kappa^2)\omega_2^2 + \omega_e^2\right]\Omega^2 + \omega_2^2 \omega_e^2}{D_1(\Omega)}, \tag{23a}$$

$$\hat{x}_d = \frac{F_0}{m_1} \frac{\Omega^2(-\Omega^2 + \omega_e^2)}{D_1(\Omega)}, \tag{23b}$$

$$\hat{\bar{Q}} = \frac{F_0}{m_1} \frac{j\kappa_2 \omega_2 \Omega^3}{D_1(\Omega)}, \tag{23c}$$

where:

$$D_1(\Omega) = -\Omega^6 + \left[\omega_1^2 + (1 + \mu)(1 + \kappa_2^2)\omega_2^2 + \omega_e^2\right]\Omega^4$$
$$- \left[(1 + \kappa^2)\omega_1^2 \omega_2^2 + \omega_1^2 \omega_e^2 + (1 + \mu)\omega_2^2 \omega_e^2\right]\Omega^2$$
$$+ \omega_1^2 \omega_2^2 \omega_e^2$$
$$+ 2j\xi_1\Omega\left(\Omega^4 - \left[(1 + \kappa^2)\omega_2^2 + \omega_e^2\right]\Omega^2 + \omega_2^2 \omega_e^2\right). \tag{24}$$

In the case of the present conservative systems, as already considered in section 2.3.2, we are interested in possible anti-resonances in the response of the primary system. Observing the numerator of $\hat{x}_1$ in equation

(23a), one can deduce that two anti-resonances $\omega_{ar,+}$, $\omega_{ar,-}$ are possible, at the frequencies:

$$\omega_{ar,\pm} = \frac{1}{\sqrt{2}}$$
$$\left[(1 + \kappa_2^2)\omega_2^2 + \omega_e^2 \pm \sqrt{\left[(1 + \kappa_2^2)\omega_2^2 + \omega_e^2\right]^2 - 4\omega_2^2 \omega_e^2}\right]^{\frac{1}{2}}, \tag{25}$$

As done for simple conservative dampers in section 2.3.2, to optimise the system, we choose to enforce one of the anti-resonance frequencies to be equal to the natural frequency ω_1 of the primary system. Enforcing $\omega_{ar,\pm} = \omega_1$ in equation (25) leads to the following conditions for ω_e:

$$\omega_e = \sqrt{\frac{\omega_1^4 - (1 + \kappa_2^2)\omega_1^2 \omega_2^2}{\omega_1^2 - \omega_2^2}}, \quad \forall \omega_2 \notin I \tag{26}$$

that is valid only if ω_2 is not in the open interval $I = \,]\omega_1/\sqrt{1 + \kappa_2^2}, \, \omega_1[$ to have a positive radicand of the square root. Consequently, in such a condition, enforcing equation (26) requires to detune the DVA of the primary system: $\omega_2 \notin I \Rightarrow \omega_2 \neq \omega_1$.

To check the efficiency of the present architecture 1, Figure 7 shows the frequency response of the primary system in several conditions: (i) alone (without any damper); (ii) coupled to only a CDVA, tuned with $\omega_2 = \omega_1$; and (iii) with both a CDVA and a C-shunt for various values of ω_2, κ_2 and with equation (26) fulfilled. One can verify that in the latter case, equation (26) enables to generate an anti-resonance at ω_1. However, for all those conditions, there is always a resonance of
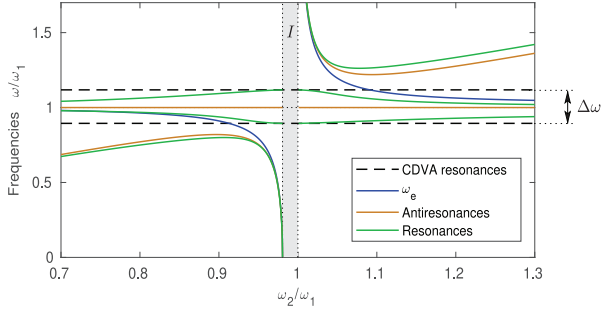
Figure 8. Resonance and anti-resonances frequencies of the frequency response of the primary mass $\hat{x}_1$ for architecture 1 as a function of the DVA natural frequency ω_2, when ω_e is chosen according to equation (26) to enforce an anti-resonance at ω_1. ω_e is also plotted (equation (26)) as well as the natural frequencies of the system with a CDVA (equation (19a)). The band gap I is specified in light gray. Mass ratio $\mu = 0.05$; coupling factor $\kappa_2 = 0.2$.

the system that is close to ω_1, inside the $\Delta\omega$ frequency band defined by the CDVA.

To verify this point, Figure 8 shows the evolution of the three resonance and the two anti-resonance frequencies of the primary mass frequency response $\hat{x}_1$ as a function of ω_2 when ω_e is chosen according to equation (26) to enforce an anti-resonance at ω_1. The band gap I is clearly visible and one can observe that for every possible tuning of the CDVA (a particular choice of ω_2), the presence of the C-shunt decreases the damping performances obtained by a single CDVA, since there is always a resonance frequency in the $\Delta\omega$ frequency band. For other value of the coupling factors μ and κ_2 than the ones chosen in Figure 8, the situation is qualitatively the same. This plot also shows that if ω_2 is in the low frequencies (lower than the band gap, $\omega_2 < \omega_1/\sqrt{1 + \kappa_2^2}$) ω_e and the two anti-resonance frequencies are also in the lower frequency band (lower than ω_1), with at the limit of I, $\omega_e = 0$. The opposite is observe for $\omega_2 > \omega_1$ in the high frequencies, with $\omega_e \to +\infty$ at the limit of I.

As a conclusion, using a C-shunt in architecture 1 is not a solution to increase the performances of a CDVA. The solution of using dissipative dampers (non-zero values of R and c_2) would lead to another situation that is out of the scope of the present article and that has been explored in (Barredo et al., 2018; Høgsberg, 2019) in the case of inerter based absorbers and piezo-electric shunts. The remaining of the article will focus on architecture 2.

4. Coupled architecture 2: EMSD between the host structure and the frame

In this section, we investigate the response and the damping performances of the second coupled DVA/EMSD architecture, shown in Figure 2(b), for which

the EMSD is placed between the primary structure and the frame. This kind of coupling seems original since, to the knowledge of the authors, no other publication consider it. We recall here that our purpose is to enhance the performance of a single DVA, described in section 2.3, by adding an EM shunt to the system. We consider here four cases, depending on the dissipative or conservative nature of the dampers. The primary structure is always considered slightly dissipative ($\xi_1 \neq 0$ is small), and coupled successively to:

- two conservative dampers: a CDVA and a C-shunt;
- a conservative mechanical damper (CDVA) coupled to a resistive shunt (R-shunt);
- a conservative mechanical damper (CDVA) coupled to a resonant shunt (RC-shunt);
- two dissipative and resonant dampers (DVA and RC-shunt).

4.1. A primary system with a CDVA and a C-shunt

We consider in this section the system of Figure 2(b) with both dampers assumed perfectly conservative, that is, with $c_2 = 0$ and $R = 0$. Keeping the notations of section 2, the governing equations of the system are:

$$(1 + \mu)\ddot{x}_1 + \mu\ddot{x}_d + 2j\xi_1\omega_1\dot{x}_1 + \omega_1^2 x_1 + \kappa\omega_1\dot{Q} = \frac{F}{m_1}, \quad (27a)$$

$$\ddot{x}_d + \ddot{x}_1 + \omega_2^2 x_d = 0, \quad (27b)$$

$$\ddot{Q} + \omega_e^2\bar{Q} - \kappa\omega_1\dot{x}_1 = 0, \quad (27c)$$

with the same variables and constants as those defined in section 2 (equations (3), (7), (9) and (15)). The frequency responses of this system can be written as:

$$\hat{x}_1 = \frac{F_0}{m_1}\frac{(\omega_e^2 - \Omega^2)(\omega_2^2 - \Omega^2)}{D_2(\Omega)}, \quad (28)$$

$$\hat{x}_d = \frac{F_0}{m_1}\frac{\Omega^2(\omega_e^2 - \Omega^2)}{D_2(\Omega)}, \quad (29)$$

$$\hat{\bar{Q}} = \frac{F_0}{m_1}\frac{j\kappa\omega_1\Omega(\omega_2^2 - \Omega^2)}{D_2(\Omega)}, \quad (30)$$

with:

$$D_2(\Omega) = -\Omega^6 + \left[(1 + \kappa^2)\omega_1^2 + (1 + \mu)\omega_2^2 + \omega_e^2\right]\Omega^4$$
$$- \left[(1 + \kappa^2)\omega_1^2\omega_2^2 + \omega_1^2\omega_e^2 + (1 + \mu)\omega_2^2\omega_e^2\right]\Omega^2$$
$$+ \omega_1^2\omega_2^2\omega_e^2$$
$$+ 2j\xi_1\omega_1\Omega(\omega_2^2 - \Omega^2)(\omega_e^2 - \Omega^2)$$

Again, like in sections 2.3.2 and 3, we are interested in creating anti-resonances in the frequency response of x_1. Observing the numerator of $\hat{x}_1(\Omega)$, it appears that

the two dampers generate two anti-resonances at their natural frequencies, at ω_2 and ω_e. We choose to tune the dampers to replace the resonance of the primary system around ω_1 by an anti-resonance. This is possible if

$$\omega_2 = \omega_1 \quad \text{or} \quad \omega_e = \omega_1 \quad\quad (31)$$

Only one of those conditions is necessary to generate the anti-resonance at ω_1.

We choose here to preserve the symmetry of the system and to generate a double anti-resonance at ω_1 by tuning the CDVA and the C-shunt so that both relations (31) are fulfilled at the same time. It is then worth predicting the location of the resonances of the system. The three eigenfrequencies of this architecture are determined by finding the zeros of $D_2(\Omega)$ with $\xi_1 = 0$, that writes in this case:

$$D_2(\Omega) = -\Omega^6 + (3 + \mu + \kappa^2)\omega_1^2\Omega^2(\Omega^2 - \omega_1^2) + \omega_1^6. \quad (32)$$

One obtains the frequencies ω_{r-}, ω_{r+} and ω_{r0}:

$$\omega_{r0} = \omega_1, \quad \omega_{r\pm} = \omega_1$$
$$\sqrt{\frac{2 + \mu + \kappa^2 \pm \sqrt{(\mu + \kappa^2)^2 + 4(\mu + \kappa^2)}}{2}}. \quad (33)$$

One of the eigenfrequencies of the system is precisely located at the anti-resonances ω_1, which means that the associated mode shape has a node at x_1: the primary mass is inert whereas the DVA and the C-shunt oscillate in phase opposition. Since, as established in section 2, the C-shunt and the CDVA are equivalent, the present case is analogous to coupling the primary structure to two identical DVAs in parallel and tuning them at the same frequency ω_1.

Figure 9 shows the frequency responses of x_1, x_d and Q for several values of the EM coupling factor κ. One can observe the double anti-resonance at $\Omega = \omega_1$ and that the qualitative behaviour of the system remains the same as with a single CDVA: the anti-resonance at ω_1 is surrounded by the two resonances at $\omega_{r\pm}$, whose frequency distance $\Delta\omega$ increases with κ. This frequency distance can be estimated by:

$$\Delta\omega \simeq \omega_1\sqrt{\mu + \kappa^2}, \quad\quad (34)$$

where the approximation holds if $\mu + \kappa^2 \ll 1$. Comparing the above equation with equation (20) as

well as the natural frequencies equation (33) with equations (19a,b) leads to conclude that the present architecture 2 is equivalent to a single damper (CDVA or C-shunt) with its coupling factor (μ or κ) replaced by $\mu + \kappa^2$. The effect of the C-shunt is thus to increase the frequency distance $\Delta\omega$, which therefore increases the performances of the CDVA (and symmetrically, the presence of the CDVA increases the performances of a single C-shunt).

Another fruitful aspect of the addition of the C-shunt is the decrease of the amplitude of x_d around the anti-resonance at ω_1: the larger the coupling factor is, the smaller the amplitude of x_d is. For applications for which large amplitudes of the CDVA are necessary at the operating point $\Omega = \omega_1$, this property is a clear advantage for the practical design of the CDVA. However, in some other applications, a given performance is targeted, measured by a given $\Delta\omega$ associated to a given value of $\mu + \kappa^2$. Then, decreasing μ by increasing κ while keeping constant their sum $\mu + \kappa^2$ will lead to a decrease of the added mass m_2 of the CDVA at constant performance $\Delta\omega$, without decreasing x_d at resonance, since exactly the same response for x_1 and x_d would be obtained (see equations (28), (29) and (32) that depend solely on $\mu + \kappa^2$). On the contrary, for a given value of μ, the normalised electric charge $\bar{Q}$ amplitude at $\Omega = \omega_1$ is almost a constant as a function of κ. Hence, enlarging $\Delta\omega$ does not imply an increase of current in the EM transducer, as long as the inductor value L is kept constant (see equation (7) for the definition of the normalised electric charge $\bar{Q}$). However, increasing κ in practice is often related to an increase of ϕ without keeping L constant (see the definition (9) of κ).

4.2. A primary system with a CDVA and a dissipative shunt

4.2.1. A primary system with a CDVA and a R-shunt.
We consider in this section the system of Figure 2(b) with the mechanical damper assumed perfectly conservative ($c_2 = 0$) and an EM resistive shunt: $C = 0$ and $R \neq 0$. The governing equations of the system are, for the mechanical part, similar to those of section 4.1: equations (27a,b), that are coupled to the one for a R-shunt defined in section 2.2: (14a).

Our reference case is the primary system coupled to the sole CDVA, that we first consider perfectly tuned, which means that $\omega_2 = \omega_1$ (see section 2.3.2). In this case, the frequency response of the primary system displacement is:

$$\hat{x}_1 = \frac{F_0}{m_1} \frac{(-\Omega^2 + \lambda_e j\Omega)(-\Omega^2 + \omega_1^2)}{-\Omega^2[\Omega^4 - (2 + \mu + \kappa^2)\omega_1^2\Omega^2 + (1 + \kappa^2)\omega_1^4] + \lambda_e j\Omega[\Omega^4 - (2 + \mu)\omega_1^2\Omega^2 + \omega_1^4]}. \quad (35)$$
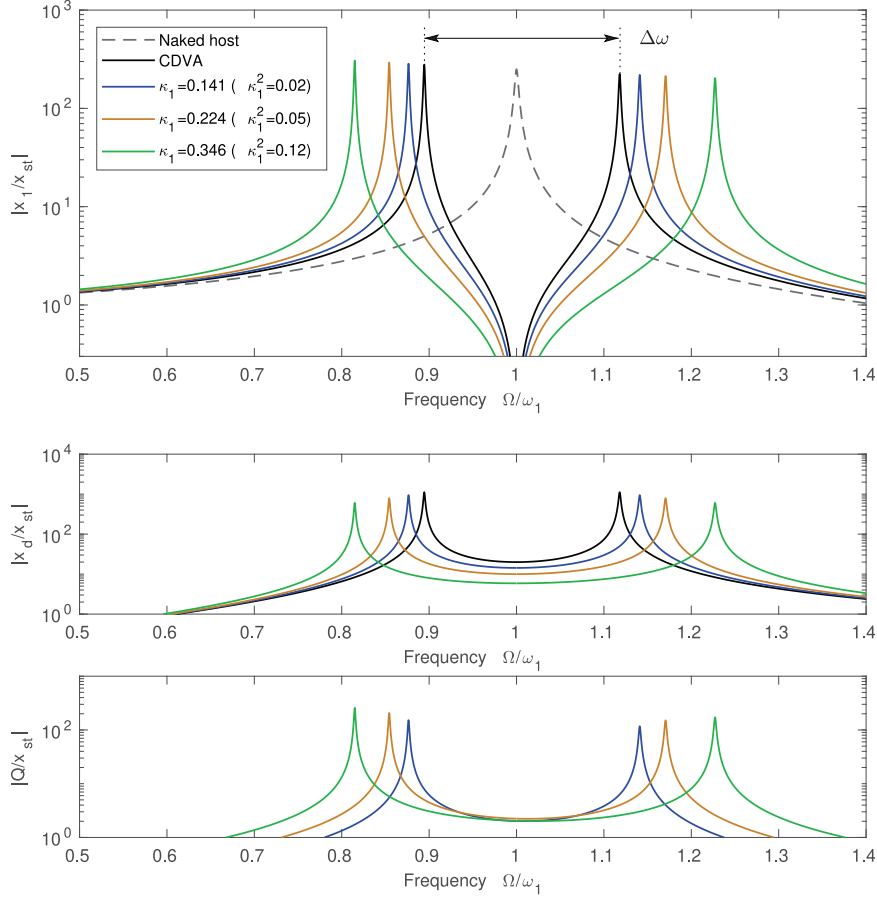
Figure 9. Frequency response $|\hat{x}_1|/|\hat{x}_1(\Omega = 0)|$ of the primary mass displacement, $|\hat{x}_d|/|\hat{x}_1(\Omega = 0)|$ of the DVA relative displacement and $|\hat{Q}|/|\hat{x}_1(\Omega = 0)|$ of the equivalent electric charge in the EM circuit, for architecture 2, with conservative dampers ($c_2 = 0$, $R = 0$), for some values of the EM coupling factor κ, as specified in the legend. The DVA natural frequency ω_2 and electrical frequency ω_e are chosen according to equation (31) to enforce a double anti-resonance at ω_1. The mass ratio is $\mu = 0.05$ and the damping ratio $\xi_1 = 0.002$.

To simplify the above expression, it has been written in the case of a conservative primary system (i.e. with $\xi_1 = 0$). Considering a nonzero ξ_1 simply adds a few terms to the denominator of $\hat{x}_1$.

This case is very similar to the canonical case of a R-shunt coupled to a simple one degree of freedom primary system, studied in section 2.3.1. Two limit cases can be considered. The first one is the case with no resistive shunt, associated to an EM transducer in open circuit ($R \to +\infty \Rightarrow \lambda_e \to +\infty$). This case has been studied in section 2.3.2 and is characterised by two resonance frequencies $\omega_{2\pm}$, defined by equation (19a). The corresponding frequency response is shown in black in Figure 10. The second limit case is the one with the EM transducer in short-circuit ($R = 0 \Rightarrow \lambda_e = 0$). In this case, the two resonances in $\omega_{2\pm}$ are shifted to the high frequencies and replaced by:

$$\omega_{sc\pm} = \omega_1 \sqrt{\frac{2 + \mu + \kappa^2 \pm \sqrt{(\mu + \kappa^2)^2 + 4\mu}}{2}}. \quad (36)$$

This case is shown in blue in Figure 10.

It can be shown that when $\xi_1 = 0$, all the curves obtained by varying the value of λ_e crosses in two fixed points, labelled F and G in Figure 10. The frequencies of those two points verify the equation $|\hat{x}_1|_{\lambda_e = 0} = |\hat{x}_1|_{\lambda_e = +\infty}$, which leads to the two frequencies (see Appendix 2):

$$\omega_{F,G} = \frac{1}{2}\omega_1 \sqrt{4 + 2\mu + \kappa^2 \pm \sqrt{(2\mu + \kappa^2)^2 + 16\mu}}. \quad (37)$$

Then, a remarkable result is that the amplitude of the frequency response at the fixed points is the same, of value :

$$|\hat{x}_1(\Omega = \omega_{F,G})| = \frac{F_0}{m_1\omega_1^2}\frac{2}{\kappa^2} \quad (38)$$

It must be noted that the above results are correct only in the case of (i) a perfectly tuned CDVA ($\omega_2 = \omega_1$) and (ii) a perfectly conservative primary system ($\xi_1 = 0$). The case of a detuned CDVA will be considered in the
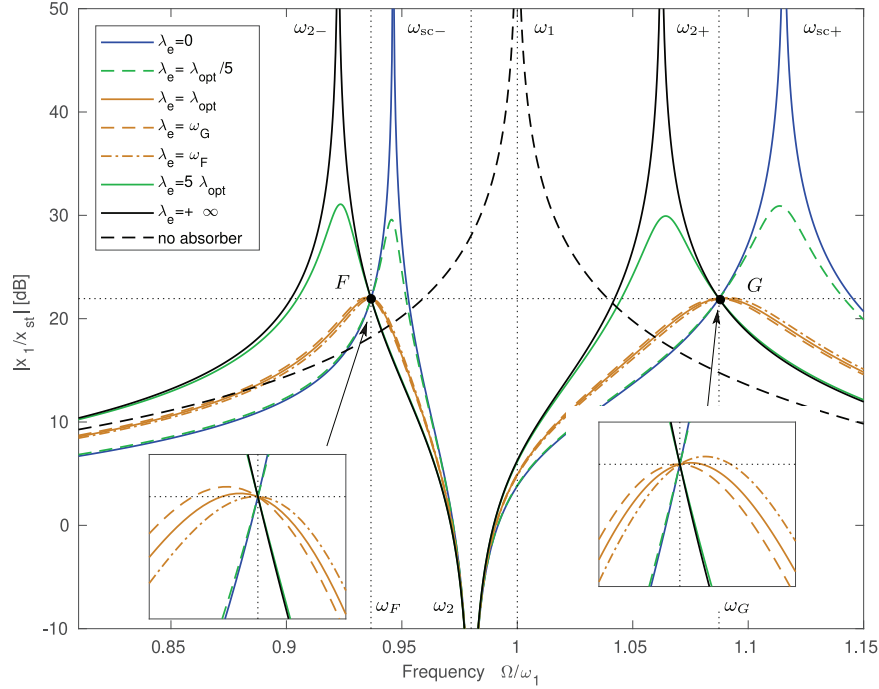
Figure 10. Frequency response $|\hat{x}_1|/|\hat{x}_1(\Omega = 0)|$ of the primary mass displacement in the case of a primary system with a CDVA and a R-shunt, for some values of the EM decay rate λ_e, as specified in the legend. The common amplitude of the fixed point is shown by a horizontal dotted line. The mass ratio is $\mu = 0.02$, the coupling factor is $\kappa = 0.4$, the damping ratio is $\xi_1 = 0$ and the CDVA frequency is $\omega_2 = 0.98\omega_1$.

following. Moreover, if $\xi_1 \neq 0$ but remain small, there are no fixed points but the overall shape of the curves remains the same.

Having in mind the above results, the H_∞ optimisation of this case is straightforward: one wants to find the value of λ_e that conducts to a frequency response with two maxima simultaneously close to F and G. As in the case of simple dissipative absorbers (single DVA or single RC-shunt, see section 2.3.1), it is not possible to have the two maxima in F and G for a single value of λ_e. However, following the result obtained for a R-shunt or a Lanchester damper (see Appendix 1; Snowdon, 1968; Thomas et al., 2012; Vakilinejad et al., 2019) for which the optimal value of λ_e is the frequency of the fixed point, one can verify by symbolic computations that taking $\lambda_e = \omega_F$ (resp. $\lambda_e = \omega_F$) leads to a $|\hat{x}_1|$ curve with a maxima at point F (resp. G). A good approximation of the optimal value $\lambda_{e,\,\text{opt}}$ of λ_e is then:

$$\lambda_e^{\text{opt}} = \sqrt{\frac{\omega_F^2 + \omega_G^2}{2}} = \omega_1\sqrt{1 + \frac{\mu}{2} + \frac{\kappa^2}{4}} \quad (39)$$

The three frequency responses (for $\lambda_e = \omega_F, \omega_G, \lambda_{e,\,\text{opt}}$) are shown in orange in Figure 10, validating qualitatively our computations.

It should be noticed that a performance indicator A_{dB}, the attenuation with respect to the naked absorber resonance, can be defined in the same way as in section 2.3.1 by equation (16). In the present case of a R-shunt coupled to a primary system and a CDVA, the common amplitude at the fixed points (equation (38)) does not depend on μ and is identical to the one for a sole R-shunt (equation (A.2)). Consequently, A_{dB} is exactly the same as in the case of a sole R-shunt and the presence of the CDVA only adds an anti-resonance to the R-shunt case, without changing its attenuation property. A_{dB} as a function of κ^2 is thus given by the red dashed curve of Figure (6), whatever be the value of μ.

Finally, another important result comes from the case for which the CDVA is detuned, namely if $\omega_2 \neq \omega_1$. This situation, shown in Figure 10, is very similar to the tuned case addressed above: there is a strict anti-resonance at $\Omega = \omega_2$ and the two fixed points F and G still exist, at frequencies:

$$\omega_{F,G} = \frac{1}{2}\sqrt{2(1+\mu)\omega_2^2 + (2+\kappa^2)\omega_1^2 \pm \sqrt{\left[2(1+\mu)\omega_2^2 + (2+\kappa^2)\omega_1^2\right]^2 - (2+\kappa^2)\omega_1^2\omega_2^2}}. \quad (40)$$

But the most interesting result is that both fixed point still have the same amplitude and that it does not depend on ω_2, which means that the common amplitude of the fixed points is still the one of equation (38), whatever be the value of ω_2. All details of the proof of this results can be found in Appendix 2

4.2.2. A primary system with a CDVA and a RC-shunt. We consider in this section the system of Figure 2(b) with the mechanical damper assumed perfectly conservative ($c_2 = 0$). The governing equations of the system are, for the mechanical part, similar to those of section 4.1 (equation (27a,b)) and the one for a RC-shunt is defined in section 2.2 (equation (14c)).

Our reference case is still the primary system coupled to the sole CDVA, but we don't consider it perfectly tuned, so that $\omega_2 \neq \omega_1$. The frequency response of the primary system displacement is:

$$\hat{x}_1 = \frac{F_0}{m_1} \frac{(-\Omega^2 + 2j\xi_e\omega_e\Omega + \omega_e^2)(-\Omega^2 + \omega_2^2)}{D_3(\Omega)}, \quad (41)$$

with

$$\begin{aligned} D_3(\Omega) = &-\Omega^6 + \left[(1+\mu)\omega_2^2 + (1+\kappa^2)\omega_1^2 + \omega_e^2\right]\Omega^4 \\ &- \left[(1+\kappa^2)\omega_1^2\omega_2^2 + (1+\mu)\omega_2^2\omega_e^2 + \omega_1^2\omega_e^2\right]\\ &\quad \Omega^2 + \omega_1^2\omega_2^2\omega_e^2 \\ &- 2j\xi_e\omega_e\Omega\left[\Omega^4 - (\omega_1^2 + (1+\mu)\omega_2^2)\Omega^2 + \omega_1^2\omega_2^2\right] \end{aligned}$$

$$(42)$$

To simplify the above expression, it has been written in the case of a conservative primary system (i.e. with $\xi_1 = 0$). Considering a nonzero ξ_1 simply adds a few terms to the denominator of $\hat{x}_1$.

This case shows similarities with the canonical case of a RC-shunt coupled to a simple one degree of freedom primary system, studied in section 2.3.1. Two independent electrical parameters have to be chosen: the electrical natural frequency ω_e and the electrical damping ratio ξ_e. To choose the first one, Figure 11 shows the evolution of the frequency response of the primary system amplitude $|\hat{x}_1|$ for several values of ω_e, for a fixed (and low value) ξ_e. It is observed that an anti-resonance is always present at $\Omega = \omega_2$, due to the CDVA, and that another anti-resonance, close to $\Omega = \omega_e$, is also present, due to the EM shunt. This is explained by the zeros of the numerator of $\hat{x}_1$ (equation (41)). Thoses anti-resonances are flanked by three resonances peaks, that degenerate to only two resonances in the particular case of $\omega_e = \omega_2$ in the case of a conservative shunt (i.e. with $\xi_e = 0$, see section 4.1). In the
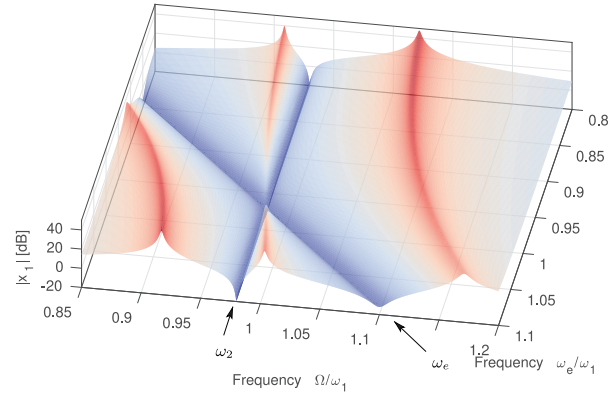

Figure 11. Frequency response $|\hat{x}_1|$ of the primary mass displacement in the case of a primary system with a CDVA and a RC-shunt, for several values of the electrical angular frequency ω_e. The CDVA angular frequency is $\omega_2 = 0.98\omega_1$, the mass ratio is $\mu = 0.01$, the coupling factor is $\kappa = 0.2$ and the damping ratios are $\xi_e = 0.005$, $\xi_1 = 0.001$ and $\xi_2 = 5 \cdot 10^{-4}$.

present case of $\xi_e \neq 0$, even if we didn't look for a mathematical proof (it would have involved computing the minima of $|\hat{x}_1|$ and verify if $\Omega = \omega_e$ is one of them), we will assume that $\omega_e = \omega_2$ still leads to the cancellation of the central resonance, which is the criteria we choose in the following to tune ω_e.

To go on, Figure 12 shows the frequency response of the primary system amplitude $|\hat{x}_1|$ for several values of ξ_e in the case of a tuned EM absorber ($\omega_e = \omega_2$). Two limit cases can be considered. The first one is the case with no resonant shunt, associated to an EM transducer in open circuit ($R \to +\infty \Rightarrow \xi_e \to +\infty$), and is characterised by two resonance frequencies $\omega_{2\pm}$. The corresponding frequency response is shown in black in Figure 12. This case is the CDVA case considered in section 2.3.2 with $\omega_2 = \omega_1$, for which $\omega_{2\pm}$ are given by equation (19a). The second limit case is the one with a conservative resonant shunt ($R = 0 \Rightarrow \xi_e = 0$), and is also characterised by two resonance frequencies $\omega_{r\pm}$. The corresponding frequency response is shown in blue in Figure 12. This case correspond to the two conservative absorbers perfectly tuned, considered in section 4.1 in the case $\omega_2 = \omega_1$, for which $\omega_{r\pm}$ are given by equation (33).

It could be shown that when $\xi_1 = 0$, all the curves obtained by varying the value of ξ_e crosses in two fixed points, labelled F and G in Figure 12, defined by the intersection of the blue and the black curves. The frequencies of those two points verify the equation $|\hat{x}_1|_{\xi_e = 0} = |\hat{x}_1|_{\xi_e = +\infty}$. To obtain the coordinates of those points, we proceed as explained in (Thomas et al., 2012) for a classical resonant shunt and we obtain for the frequencies (see Appendix 3):

$$\omega_{F,G} = \frac{1}{2}\sqrt{2(1+\mu)\omega_2^2 + (2+\kappa^2)\omega_1^2 \pm \sqrt{\left[(2(1+\mu)\omega_2)^2 + (2+\kappa^2)\omega_1^2\right]^2 - 16\omega_1^2\omega_2^2}} \quad (43)$$
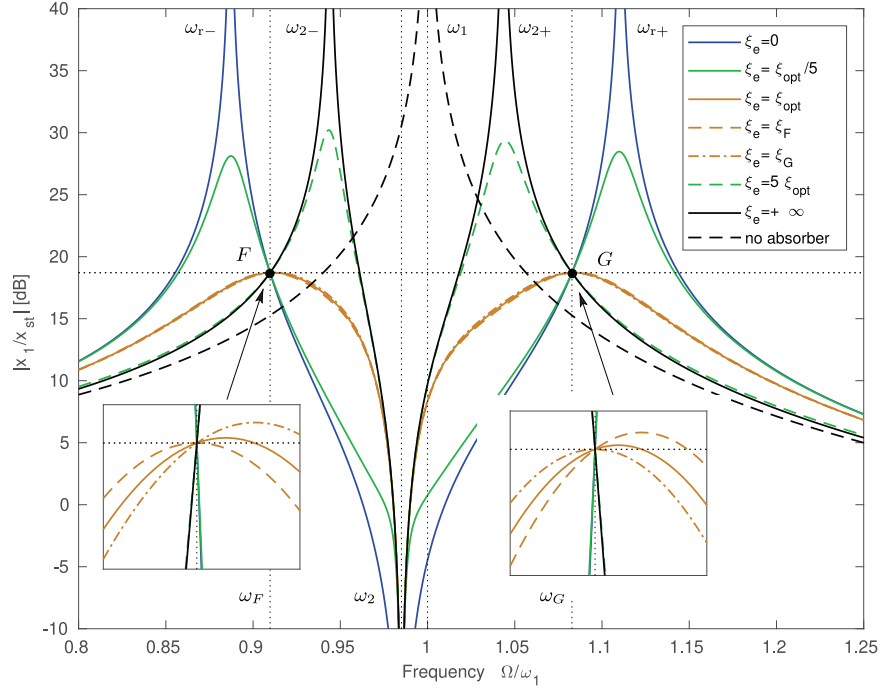
Figure 12. Frequency response $|\hat{x}_1|/|\hat{x}_1(\Omega = 0)|$ of the primary mass displacement in the case of a primary system with a CDVA and a RC-shunt, with tuned absorbers $\omega_e = \omega_2 = \omega_e$ and for some values of the EM damping ratio ξ_e, as specified in the legend. The amplitudes of the fixed point F an G are shown by a horizontal dotted lines. The mass ratio is $\mu = 0.01$, the coupling factor is $\kappa = 0.2$ and the damping ratio $\xi_1 = 0$.

One can verify that the corresponding amplitudes of $|\hat{x}_1|$ are not equal and that their relative location depends on ω_2. It is thus possible to find a value ω_2^{opt} that guarantee two equal amplitude for the fixed points F and G. As shown in Appendix 3, we obtain:

$$\omega_2^{\text{opt}} = \omega_1 \sqrt{\frac{2 - \kappa^2}{2(1 + \mu)}}. \tag{44}$$

This value is different from $\omega_2^{\text{opt}} = \omega_1$ (only slightly since κ and μ are small in practice), which means that the present optimisation of the CDVA with the RC-shunt imposes to slightly detune the CDVA from ω_1. Then, imposing $\omega_2 = \omega_2^{\text{opt}}$ leads to:

$$\omega_{F,G}^{\text{opt}} = \omega_1 \sqrt{1 \pm \sqrt{\frac{\kappa^2 + 2\mu}{2(1 + \mu)}}}, \tag{45}$$

for the frequencies of the fixed points and

$$|\hat{x}_1(\Omega = \omega_{F,G}^{\text{opt}})|$$
$$= \frac{F_0}{m_1\omega_1^2} \frac{2}{\kappa^2} \frac{(1 + \mu)\sqrt{2(\kappa^2 + 2\mu)} - (\kappa^2 + 2\mu)\sqrt{1 + \mu}}{(1 + \mu)\left[\sqrt{2(\kappa^2 + 2\mu)} - 2\sqrt{1 + \mu}\right]} \tag{46}$$

for their common amplitude.

Then, the H_∞ optimisation of this case is straightforward: one wants to find the value of ξ_e that conducts to a frequency response with two maxima simultaneously close to F and G. As in the case of simple dissipative absorbers (single DVA or single RC-shunt, see section 2.3.1, or the previous case of section 4.2.1), if $\xi_1 = 0$, it is not possible to have the two maxima in F and G for a single value of ξ_e. Symbolic manipulation lead to very complex analytical expressions for $\xi_{F,G}^{\text{opt}}$ (the value of ξ_e for which a maxima occurs in F, G) and their mean value $\xi_e^{\text{opt}} = (\xi_F^{\text{opt}} + \xi_G^{\text{opt}})/2$, that we where not able to simplify. Only a graphical plot is reported here, as the contour lines of Figure 13. Here, a simplified expression of ξ_e^{opt} when μ and κ are small seems not convenient, due to its non monotonous shape of the function $\xi_e^{\text{opt}} = f(\mu, \kappa^2)$, especially as a function of μ for a fixed κ (remark the curved contour lines in Figure 13). The corresponding frequency responses are shown in orange in Figure 12, showing that ξ_e^{opt} is a good approximation of the optimal electrical damping for a H_∞ optimisation.

4.3. A primary system with two resonant dissipative dampers

Now, we investigate the combination of a two dissipative resonant dampers, a DVA and a RC-shunt, coupled to a primary system, as shown in Figure 2(b).
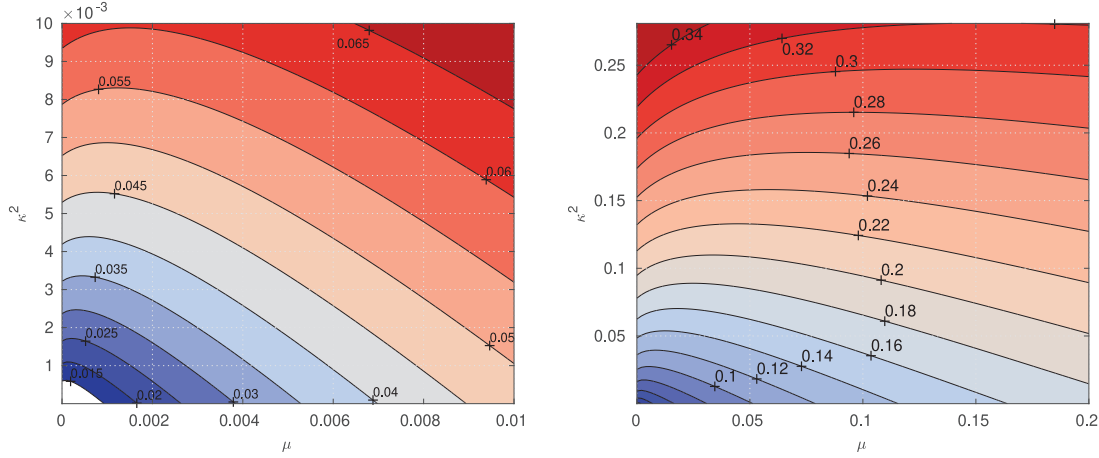
Figure 13. Contour lines of the optimal electrical damping ratio ξ_e^{opt} as a function of the mass ratio μ and the coupling factor κ^2, in the case of a conservative primary system ($\xi_1 = 0$) with a CDVA and a RC-shunt.

The governing equations of this system are the following set of equations:

$$(1 + \mu)\ddot{x}_1 + \mu\ddot{x}_d + 2\xi_1\omega_1\dot{x}_1 + \omega_1^2 x_1 + \kappa\omega_1\dot{Q} = \frac{F}{m_1}, \quad (47)$$

$$\ddot{x}_d + \ddot{x}_1 + 2\xi_2\omega_2\dot{x}_d + \omega_2^2 x_d = 0, \quad (48)$$

$$\ddot{Q} + 2\xi_e\omega_e\dot{Q} + \omega_e^2\bar{Q} - \kappa\omega_1\dot{x}_1 = 0. \quad (49)$$

In this case, it would be interesting to investigate the optimal tuning of both dampers to obtain a maximum amplitude attenuation effect. Since both dampers are dissipative, one has to find the optimal value of four parameters: (ω_2/ω_1, ω_e/ω_1, ξ_2, ξ_e) as a function of μ, κ and ξ_1. This work is left apart from the present article and we just give here some results obtained by numerical trial and error investigations.

First, we remarked that with both dissipative dampers, the fixed point property seems lost: when ξ_2 and ξ_e are varied with $\omega_e = \omega_2$, there is no more fixed point that appear. Then, Figure 14 gives the primary mass frequency response $\hat{x}_1$ in the case of an optimally tuned DVA + RC-shunt situation, obtained by varying $\omega_e = \omega_2$, ξ_e and ξ_2. It appears that a good resonance attenuation is obtained.

4.4. Comments on architecture 2. Observing Figures 10 and 12 leads to evaluate the benefit of adding a dissipative shunt (R-shunt or RC-shunt) to a conservative DVA. The presence of the shunt does not alter any benefit of having a conservative DVA since it keeps the anti-resonance. It just helps to attenuate the negative effects of the two side resonances, with a more pronounced effect with the RC-shunt. This can be observed in Figure 14 where a gain of about 15 dB is obtained between the maxima of the frequency responses of the R-shunt and RC-shunt coupled to the CDVA, with $\mu = 0.01$ and $\kappa = 0.2$. This figures also lead to conclude

that the benefit of two dissipative absorbers (a DVA and a RC-shunt) does not bring a large improvement of the vibratory behaviour corresponding to the case of a conservative mechanical absorber (CDVA) plus a resistive shunt (RC-shunt). It only slightly reduces the maxima (of about 2.4 dB) with the drawback of completely eliminating the anti-resonance. The CDVA + RC-shunt configuration seems then very interesting for application for which the amplitude of vibration must be drastically reduced in a narrow frequency band, without increasing so much the amplitude in the side resonances.

5. Experiments

This section aims at presenting an experimental validation of the theoretical results exposed in the previous sections. Only architecture 2 of Figure (2b), addressed in section 4, is considered here, since it has been shown that architecture 1 is less interesting than architecture 2 in practice.

5.1. Experimental setup

An electromagnetic transducer in the form of a voice coil (VCA, model PKM 1715, Pack Aero, France), shown in Figure 15, enabled to couple the vibrations of the structure to an electronic circuit (labelled 'shunt'). It is composed of a coil in the form of a solenoid, fixed to the upper plate of the structure, free to move in a radial magnetic field created by a permanent magnet clamped to the frame. The measured electrical characteristics of the VCA are following: inductance $L = 664\mu H$, internal resistance $R_L = 3.2\Omega$ and force factor $\phi = 2.98N/A$ (see Figures 16 and 19 for the equivalent model of the EM transducer). The first two were estimated by an impedance measurement. To measure the force factor, a voltage signal $V(t)$ was imposed to the terminals of
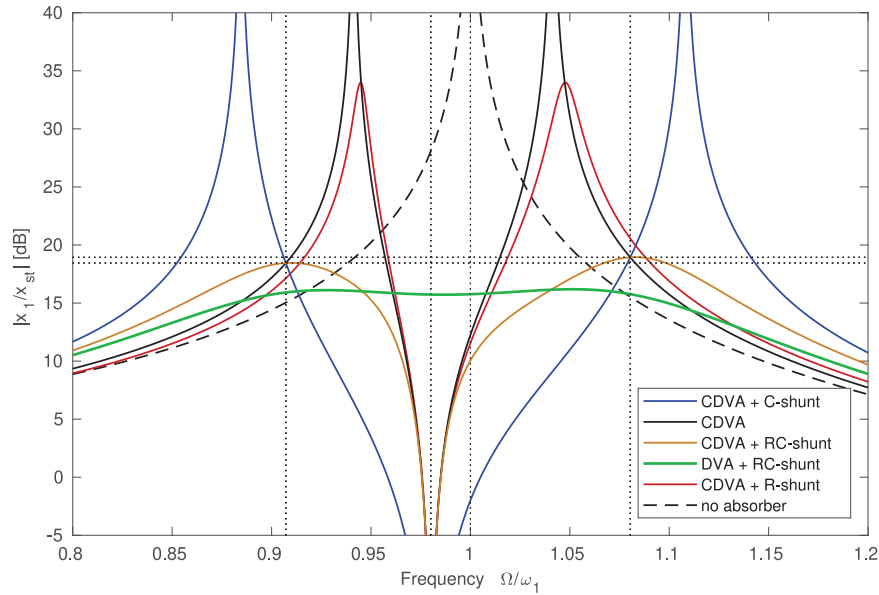
Figure 14. Frequency response $|\hat{x}_1|/|\hat{x}_1(\Omega = 0)|$ of the primary mass displacement in the case of a primary system with a DVA and a RC-shunt optimally tuned (green curve), compared to other dampers, as specified in the legend. All dampers are tuned with $\omega_2 = 0.98\omega_1$, which gives the best optimisation for the DVA + RC-shunt situation. $\xi_e = 0.154$ in this latter situation. The electrical frequency is $\omega_e = \omega_2$ in all cases and the mass ratio is $\mu = 0.01$, the coupling factor is $\kappa = 0.2$ and the damping ratio $\xi_1 = 0$.
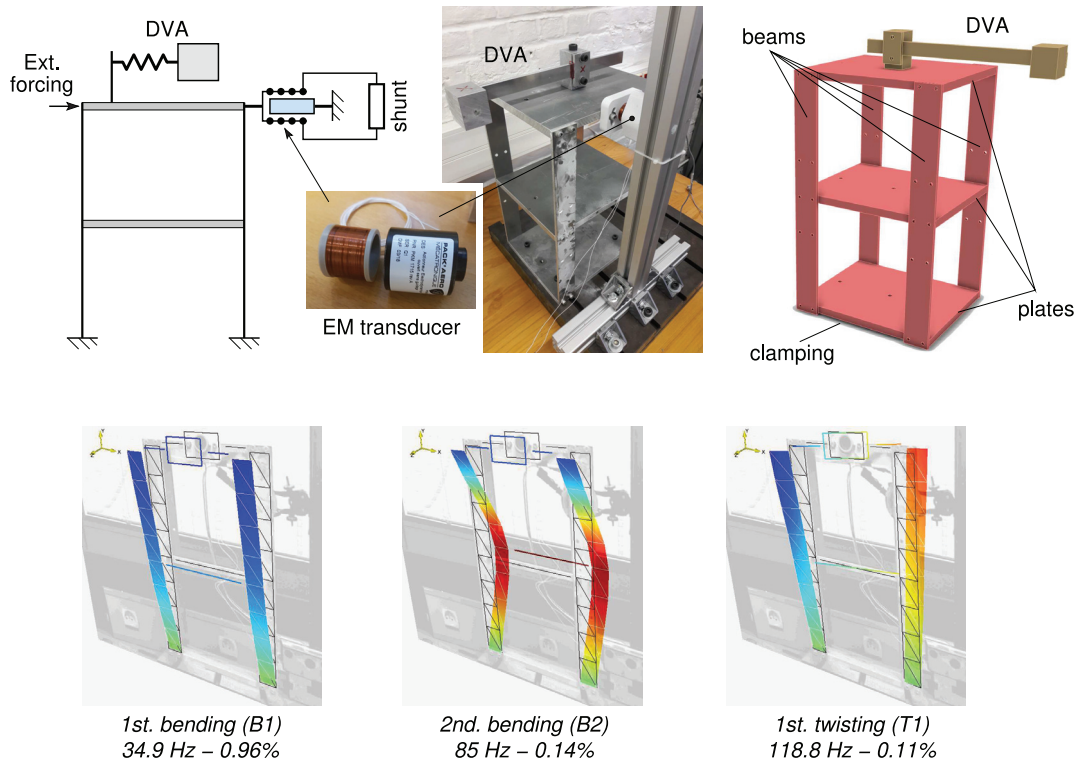

Figure 15. Scheme, picture and CAD view of the structure under test and the EM transducer. Three first eigenmodes of the 'naked' structure, without the DVA and the transducer, measured with a laser vibrometer (Polytec PSV-400).

the coil and the corresponding differential mechanical velocity $v(t)$, between the coil and the magnet, was measured. A plateau in the modulus of the frequency response function $\hat{V}/\hat{v}$ leaded to the value of ϕ.

A mechanical DVA could also be added to the top of the structure, in the form of a cantilever beam with a mass fixed at its free end. The beam acts as a spring and the end mass as an inertia. The clamping of the DVA to
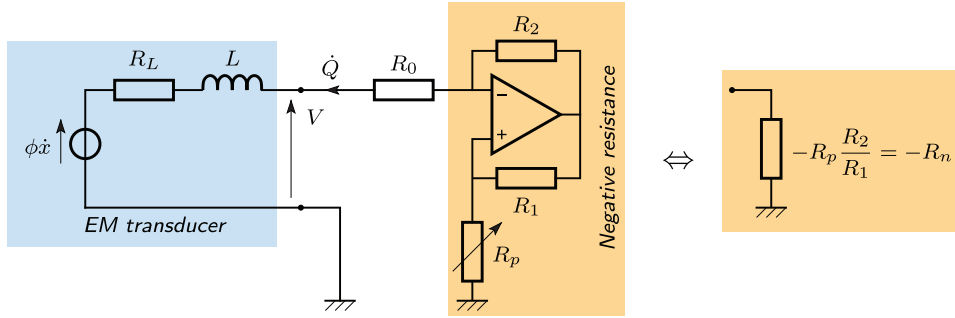
Figure 16. Electronic circuit used to create the resistive shunt, including a negative resistance realised with an operational amplifier. The electromagnetic transducer is classically modelled as an inductor L in series with an internal resistance R_L and an electromotive force $\phi\dot{x}$.

Table 2. Geometrical and material details of the components of the host structure.

	Mass [g]	Length [m]	Width/external diameter [m]	Thickness [m]
Plate	1628	240	200	12
Beam	219.4	400	40	5
Coil assembly*	42.1	25.9	26	–
Magnet assembly*	131.6	35	29.8	–
Exciter magnet	6	10	10	–
DVA built	161.1	–	–	–
DVA mobile mass	149.8	40	40	34
DVA beam	48.7	⩽300	20	3

* The measured mass is the mass of the item and its fixture.

the top plate of the structure was designed to adjust the desired length of the beam to tune the stiffness of the DVA on a particular frequency. The whole device was carefully machined so that the equivalent damping ratio of the DVA was very weak (of the order of 0.45%), to obtain a device as close as possible to a conservative DVA (CDVA).

5.2. Results with an analog resistive shunt

The first test reported in this article is the simplest shunt that can be realised: a simple resistive shunt. Using the optimal value of the electrical time constant λ_e^{opt} of Table 1, it was possible to obtain the optimal value of the shunt resistance R. Remember that R refers to the whole resistance of the circuit and that it thus includes R_L. We obtained 0.145Ω for mode B_1 and 0.355Ω for mode B_2 (see Table 3), which is less than the internal resistance of the coil $R_L = 3.2\Omega$. Consequently, it was necessary to artificially lower the resistance of the shunt circuit. As a proof of concept, we present in this section the use of a synthetic negative resistance realised by an analog electronic circuit, based on an operational amplifier (op-amp). The circuit is shown in Figure 16. If the op-amp is assumed perfect, the equivalent impedance of the circuit of Figure 16 is $-R_n < 0$ with $R_n = R_p R_2/R_1 > 0$, where R_2 and R_2 are two fixed

resistors and R_p is a tunable resistor, made with potentiometers, used to adjust the value of the equivalent negative capacitance R_n. Since this component can become unstable if the negative resistance becomes larger in absolute value than the resistance of the circuit, which is small ($\simeq 3.5\Omega$), we added a larger positive resistance $R_0 = 28\Omega$ in series in the circuit to facilitate the experimental tuning of the negative resistance.

An experimental structure, shown in Figure 15, was designed to test the vibration absorber concepts presented in the previous sections. It is composed of three identical plates, the bottom one being clamped to a frame, sustained by four identical beams, all built in aluminium. The geometrical characteristics (see Table 2) were chosen to obtain a structure for which its two first vibration modes are two bending modes (modes B_1 and B_2 in Figure 15) with the twisting modes (the first one being mode T_1 in Figure 15) shifted to higher frequencies. A coil magnet exciter (with a fixed coil and a small cylindrical magnet glued on one of the vertical beams, not shown in Figure 15, see Thomas et al. (2003) for details) was used to drive in vibrations the structure. Measuring the current intensity signal $I_{\mathrm{drive}}(t)$ in this coil, assumed proportional to the force applied to the structure, gave a reference for the frequency response functions measured in the experiments presented in this article.
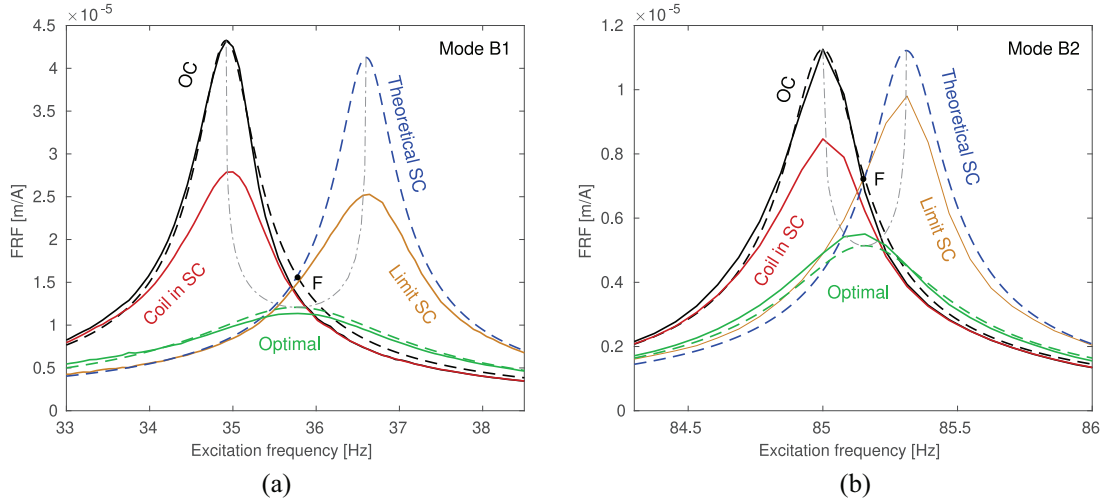
Figure 17. Experimental frequency response $|\hat{x}_1/\hat{I}_{\text{drive}}|$ of the structure coupled to a resistive electromagnetic shunt (R-shunt), with the negative capacitance realised with the analog circuit of Figure 16. (a): R-shunt tuned to mode B_1; (b) R-shunt tuned to mode B_2.

The frequency response of the structure with a resistive shunt is shown in Figure 17 for several values of the resistance of the shunt. The velocity $\dot{x}_1$ of the top plate of the structure was measured by a laser vibrometer and the reference signal was the current intensity in the driving coil I_{drive}. The open circuit condition (OC) was obtained by leaving the terminals of the coil open. Since no current flows in the coil, it corresponds to the natural response of the structure. Then, short circuiting the coil is equivalent to impose a shunt resistance R equal to $R_L = 3.5\Omega$, the internal resistance of the coil. This case is shown in red in Figure 17. In addition, by increasing the negative capacitance R_n from zero, it was possible to obtain an optimal response for the system (in green), the response with the lowest amplitude. Increasing further R_n and thus lowering the whole resistance in the circuit until the limit of stability, it was possible to reach the orange (Limit SC) curve. Finally, the blue dashed curve gives the theoretical response of the system if it had been possible to fully cancel the internal resistance of the coil, to obtain a theoretical $R = 0$ shunt resistance. The theoretical locus of the peak amplitude of the response when R is varied is shown in dashed grey showing an excellent agreement with theory (Figure 4), especially with the peak of the optimal curve being located just below the fixed point F because of the nonzero damping ξ_1.

In the present case, because of the high internal resistance of the EM transducer, it was not possible to estimate directly the EMCF with equation (13) as it is traditionally done for piezoelectric transducers (see e.g. Thomas et al., 2012), since $\omega_{1,\text{sc}}$ is defined as the natural frequency of the system short circuited with a perfectly zero shunt resistance $R = 0$, the blue curves of
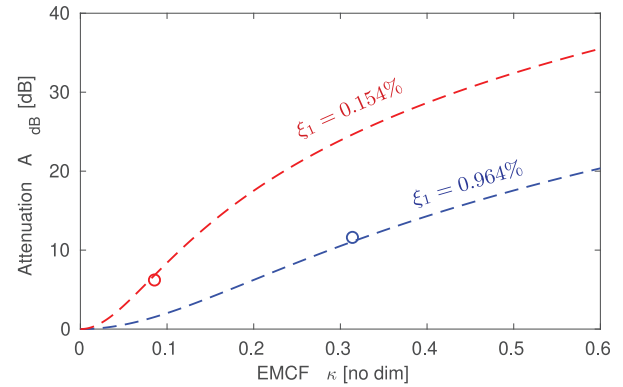

Figure 18. Attenuation A_{dB} due to R-shunt as a function of the EMCF κ, for values of eigenmodes damping ξ_1, for mode B_1 and B_2. Theory from section 2.3.1 and Figure 6 is in solid line and experimental values are shown by points.

Figure 17(a) and (b), which is here only theoretically predicted. However, using the experimental value of R obtained for the optimal situation of Figure 17 (green curves), one can deduce λ_e^{opt} with Table 1 and obtain κ by:

$$\kappa \simeq \sqrt{2\frac{(\lambda_e^{\text{opt}})^2 - \omega_1^2}{\omega_1^2}}. \tag{50}$$

The two estimated values of κ are 0.314 and 0.085 for mode B_1 and B_2, respectively, as indicated in Table 3.

Finally, considering these experimental values κ and the ones of ξ_1 (see Table 3), it is possible to compare the attenuation A_{dB} brought by the resistive shunt between experiments and theory, see Figure 18. In

Table 3. Experimental modal characteristics of the structure (three first lines) and theoretical optimal values of the electrical parameters, obtained by the equations of Table 1 for the R-shunt and RC-shunt, equation (39) for the CDVA + R-shunt and equation (44) and Figure (13) for the CDVA + RC-shunt, together with equation (15) to obtain R_{opt} and C_{opt}.

		Analog shunt		Digital shunts				
		R-shunt Mode B₁ Figure 17(a)	Mode B₂ Figure 17(b)	R-shunt Mode B₁ Figure 20(a)	RC-shunt Mode B₁ Figure 20(a)	CDVA + C-shunt Mode B₁ Figure 20(b)	CDVA + R-shunt Mode B₁ Figure 20(c)	CDVA + R-shunt Mode B₁ Figure 20(d)
Natural frequency (OC) $\omega_1/(2\pi)$	[Hz]	34.9	85.0	33.3	33.3	33.3	33.3	33.3
Damping ξ_1	[%]	0.964	0.154	0.728	0.728	0.728	0.728	0.728
EMCF κ	[–]	0.314	0.085	0.24	0.24	0.24	0.24	0.24
Optimal electrical time const. λ_e^{opt}/ω_1	[–]	1.024	1.002	1.014	–	–	1.02	–
Optimal electrical damping ξ_e	[–]	–	–	–	0.147	0	–	0.17
Optimal resistance R_{opt}	[Ω]	0.145	0.355	0.141	0.04	0	0.142	0.045
Optimal electrical frequency ω_e^{opt}	[Hz]	–	–	–	32.8	33.3	–	32.03
Optimal capacitance C_{opt}	[mF]	–	–	–	35	34	–	37

regards to those graphs, we can conclude a good agreement between this experimental values and the theory, that validate this R-shunt and its application.

5.3. Results with a digital shunt

Because we are interested in validating resonant shunts, we also need to add a capacitor C in the circuit. Following Table 1, the electric natural frequency $\omega_e = 1/\sqrt{LC}$ of the resonant shunt has to be chosen very close to the natural frequency of the targeted mode of the primary system. To target the resonance of the first mode $f_1 = \omega_1/(2\pi) = 33.3Hz$ with a coil inductance $L = 664\mu H$, the optimal value of the capacitance is $C \simeq 35mF$. Since this value is huge for a simple electronic component, we chose to synthesise it. Otherwise, it would require the use of an electrolytic capacitor for which a bias voltage would be necessary to avoid bipolar voltages. Moreover, since we also need a negative resistance in the shunt, using an op-amps based electronic circuit was found difficult to master and we chose to test another strategy: the use of a real time digital controller (RTC). In this case, both the negative resistance and the capacitance were simulated by the RTC.

The electronic circuit is shown in Figure 19. Since the RTC (a dSPACE MicroLabBox DS1202) is used to simulate a particular impedance, its input should be the current in the circuit and its output a voltage. Consequently, the input of the RTC is connected to the shunt through a current measurement circuit, built with a Texas Instrument OPA445 op-amp. It is an inverting amplifier of gain -1 (because the same resistance $R_4 = 74.9\Omega$ is used at the inverting input and for the negative feedback) which delivers an input voltage to the RTC $V_{ADC} = -R_m I$, with $I = \dot{Q}$ the current intensity in the shunt. Knowing the measuring resistance $R_m = 28.4\Omega$ enables to obtain an input proportional to I. At the output of the RTC, a voltage follower is used, built with a second op-amp (a Texas Instrument OPA547T). The two op-amps are supplied by a DC power supply (FI 1333, Française d'Instrumentation, France). Finally, the RTC was programmed to simulate an impedance equivalent to:

$$Z_{RTC} = -R_n + \frac{1}{jC\Omega}. \tag{51}$$

The sampling frequency of the RTC is 30 kHz, which is enough for the frequency band of interest of our structure, with the second mode at about 85 Hz.

Using the above described digitally synthesised shunt, we tested four shunt configurations. For each configuration, the mechanical frequency response $|\hat{x}_1/\hat{I}_{drive}|$ of the structure was measured in the same way than in the previous section. Figure 20(a) shows the results for the first configuration: a sole EM shunt.
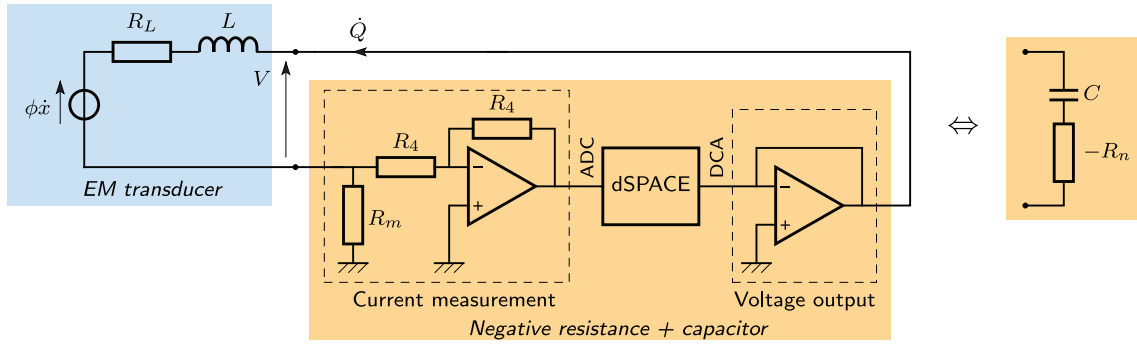
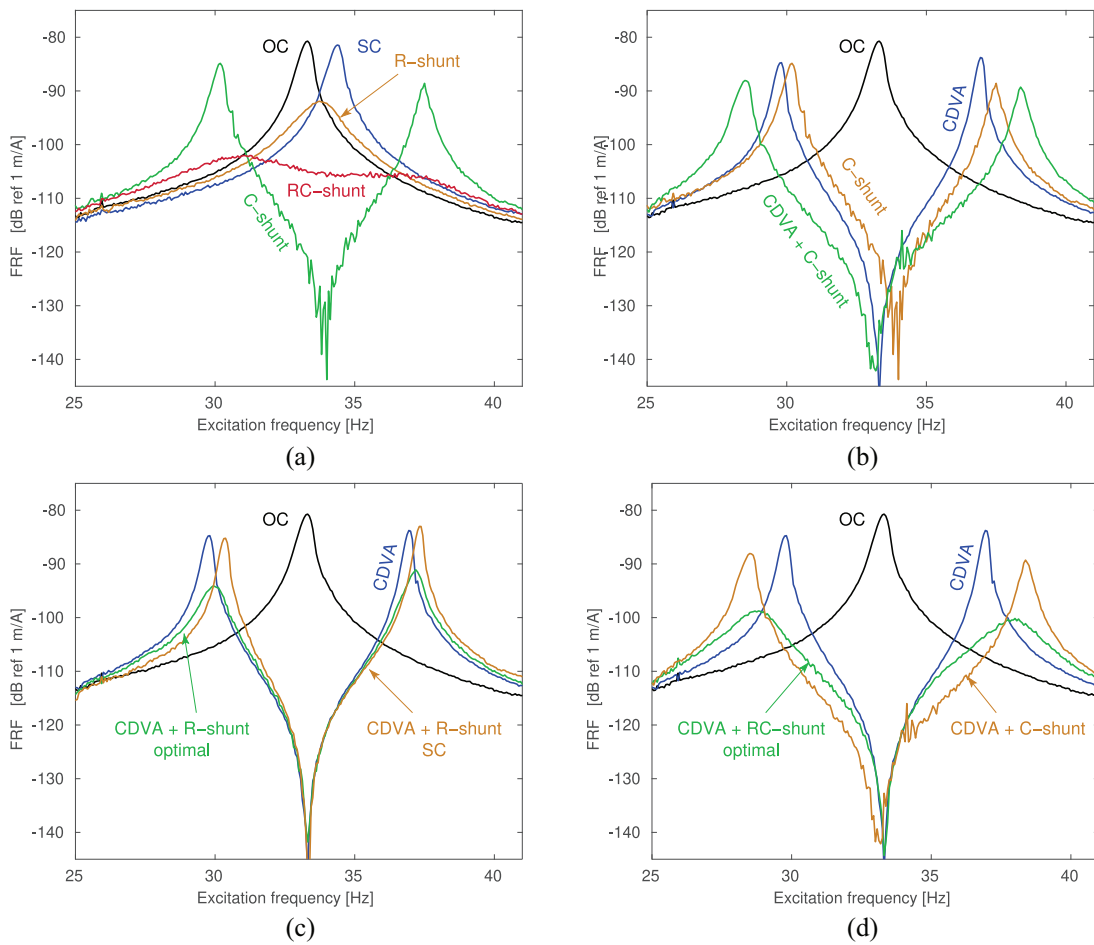**Figure 19.** Electronic circuit used to synthetise a resonant shunt with dSpace.

Figure 20. Experimental frequency response $|\hat{x}_1/\hat{I}_{\text{drive}}|$ of the structure coupled to several shunt configurations realised with a real-time controller, around mode B_1 resonance. (a) primary structure coupled to a single EM shunt absorber (R-shunt, RC-shunt and C-shunt are shown); (b) primary structure coupled to a CDVA and a C-shunt; (c) primary structure coupled to a CDVA and a R-shunt; (d) primary structure coupled to a CDVA and a R-shunt. The electromechanical coupling factor is $\kappa = 0.24$ and the CDVA mass ratio is $\mu = 0.05$.

All possible configuration are shown optimally tuned: a R-shunt, a C-shunt and a RC-shunt. An excellent agreement with theory is obtained since the curves cross each other at the particular fixed points (see section 2.3 for details). In particular, one can remark the creation

of a remarkable anti-resonance in the case of the C-shunt, for which the negative capacitance R_n has been increased to be as close as possible to the instability limit. Another remark is that the RC-shunt is slightly detuned with respect to the perfect equal peak

situation, since the same electrical frequency ω_e (and thus the same value of C) as in the C-shunt case has been used, that is, $\omega_e = \omega_1$. Considering theory, the RC-shunt has to be slightly detuned with respect to ω_1 to be optimal ($\omega_e^{\text{opt}} = \omega_1 \sqrt{(2 - \kappa^2)/2}$, see Table 1) and to have the two fixed points at the same amplitude.

Figure 20(b)–(d) show the frequency response of the structure coupled to a CDVA and various shunts (a C-shunt, a R-shunt and a RC-shunt). For the three situations, the CDVA is tuned to create an anti-resonance in place of the primary system resonance $\omega_2 = \omega_1$. For the C-shunt and the RC-shunt, the electrical frequency is also tuned in the same way, so that $\omega_e = \omega_2 = \omega_1$. An excellent agreement is obtained with the theory exposed in section 4: Figure 20(b)–(d) can be compared to their theoretical counterparts, Figures 9, 10 and 12. It is remarkable to observe that the theoretical fixed points are present as predicted by theory. Moreover, in the case of Figure 20(b), the addition of the C-shunt to the CDVA increases the distance between the two resonances, while keeping the anti-resonance, as predicted by theory. For Figure 20(d), since the tuning is $\omega_e = \omega_2 = \omega_1$, it is not optimal and we can observe that the left (low frequency) fixed point has an amplitude slightly higher than the right (high frequency) one. A right tuning would have been to slightly detune $\omega_e = \omega_2$ with respect to ω_1 (see equation (44)) to obtain the two fixed points at the same amplitude.

6. Conclusion

This article presented the possible performance enhancement of a classical dynamic vibration absorber (DVA) using an electromagnetic (EM) shunt. The focus was on the use of a conservative DVA (CDVA), because of its property to create a strict anti-resonance at its natural frequency. It was shown that the addition of an EM shunt does not break this remarkable property, even if it is dissipative. Moreover, it was shown that a properly tuned EM shunt was able to substantially damp the two adjacent resonances of the CDVA, thus obtaining a damping system able to create an anti-resonance without creating sharp anti-resonances. It was also discovered that fixed points are also present in the frequency response of a CDVA with an EM-shunt, enabling to derive simple analytical formulae, giving a clear design methodology for this kind of coupled absorbers.

Declaration of conflicting interests

The author(s) declared no potential conflicts of interest with respect to the research, authorship and/or publication of this article.

ORCID iD

Olivier Thomas (iD) https://orcid.org/0000-0001-7240-5259

References

ANSI/IEEE Std 176-1987 (1988) *IEEE Standard on Piezoelectricity*. Newtork: The Institute of Electrical and Electronics Engineers, Inc.

Ao WK and Reynolds P (2019) Evaluation of optimal analysis, design, and testing of electromagnetic shunt damper for vibration control of a civil structure. *Structural Control Health Monitoring* 27(3): e2495.

Ao WK and Reynolds P (2020) Analysis and numerical evaluation of h_∞ and h_2 optimal design schemes for an electromagnetic shunt damper. *Journal of Vibration and Acoustics* 142(2): 021003.

Asai T, Araki Y and Ikago K (2017) Energy harvesting potential of tuned inertial mass electromagnetic transducers. *Mechanical Systems and Signal Processing* 84: 659–672.

Bae J-S, Hwang J-H, Roh J-H, et al. (2012) Vibration suppression of a cantilever beam using magnetically tuned-mass-damper. *Journal of Sound and Vibration* 331: 5669–5684.

Barredo E, Blanco A, Colín J, et al. (2018) Closed-form solutions for the optimal design of inerter-based dynamic vibration absorbers. *International Journal of Mechanical Sciences* 144: 41–53.

Behrens S, Fleming AJ and Moheimani SOR (2003) Electromagnetic shunt damping. In: *Proceedings of the 2003 IEEE/ASME international conference on advanced intelligent mechatronics (AIM 2003)*, Vol. 2, pp. 1145–1150. Kobe, Japan: IEEE.

Berardengo M, Thomas O, Giraud-Audine C, et al. (2016) Improved resistive shunt by means of negative capacitance: new circuit, performances and multi-mode control. *Smart Materials and Structures* 25(7): 075033.

Bourquin F, Caruso G, Peigney M, et al. (2014) Magnetically tuned mass dampers for optimal vibration damping of large structures. *Smart Materials and Structures* 23: 085009.

Brock JE (1946) A note on the damped vibration absorber. *Journal of Applied Mechanics* 68: A–284.

Busch-Vishniac I (1999) *Electromechanical Sensors and Actuators*. Newyork: Springer.

Caruso G (2001) A critical analysis of electric shunt circuits employed in piezoelectric passive vibration damping. *Smart Materials and Structures* 10(5): 1059–1068.

Cheng TH and Oh IK (2009) A current-flowing electromagnetic shunt damper for multi-mode vibration control of cantilever beams. *Smart Materials and Structures* 18: 095036.

Chung L-L, Lai Y-A, Yang C-S, et al. (2013) Semi-active tuned mass dampers with phase control. *Journal of Sound and Vibration* 332: 3610–3625.

Connor J and Laflamme S (2014) *Structural Motion Engineering*. Switzerland: Springer.

Ducarne J, Thomas O and Deü J-F (2010) Structural vibration reduction by switch shunting of piezoelectric elements: modelling and optimization. *Journal of Intelligent Materials Systems and Structures* 21(8): 797–816.

Elliott SJ and Zilletti M (2014) Scaling of electromagnetic transducers for shunt damping and energy harvesting. *Journal of Sound and Vibration* 333: 2185–2195.

Firestone FA (1933) A new analogy between mechanical and electrical systems. *The Journal of the Acoustical Society of America* 4: 249–267.

Forward RL (1979) Electronic damping of vibrations in optical structures. *Applied Optics* 18(5): 690–697.

Frahm H (1911) *Device for Damping Vibrations of Bodies* (Technical Report No. 989958, U.S. Patent).

Graves KE, Toncich D and Iovenitti PG (2000) Theoretical comparison of motional and transformer emf device damping efficiency. *Journal of Sound and Vibration* 233(2): 441–453.

Hagood NW and Von Flotow A (1991) Damping of structural vibrations with piezoelectric materials and passive electrical networks. *Journal of Sound and Vibration* 146(2): 243–268.

Hartog JPD (1956) *Mechanical Vibrations*. Newyork: McGraw-Hill.

Høgsberg J (2019) Vibration control by piezoelectric proof-mass absorber with resistive-inductive shunt. *Mechanics of Advanced Materials and Structures* Epub ahead of print 22 January 2019. DOI: 10.1080/15376494.2018.1551587.

Høgsberg J (2020) Consistent frequency-matching calibration procedure for electromechanical shunt absorbers. *Journal of Vibration and Control* 26(13-14): 1133–1144

Inoue T, Ishida Y and Sumi M (2008) Vibration suppression using electromagnetic resonant shunt damper. *Journal of Vibration and Acoustics* 130(041003): 1–8.

Krenk S (2005) Frequency analysis of the tuned mass damper. *Journal of Applied Mechanics* 72: 936–942.

Krenk S and Høgsberg J (2016) Tuned resonant mass or inerter-based absorbers: unified calibration with quasi-dynamic flexibility and inertia correction. *Proceedings of the Royal Society A* 472(2185): 20150718.

Lanchester FW (1914) *Damping Torsional Vibrations in Crank Shafts* (Technical Report No. 1085443, U.S. Patent).

Liu K and Liu J (2005) The damped dynamic vibration absorbers: revisited and new result. *Journal of Sound and Vibration* 284: 1181–1189.

Liu Y, Lin C-C, Parker J, et al. (2016) Exact h2 optimal tuning and experimental verification of energy-harvesting series electromagnetic tuned-mass dampers. *Journal of Vibration and Acoustics* 138: 061003.

Maxwell JC (1865) A dynamical theory of the electromagnetic field. *Transactions of the Royal Society of London* 155: 459–512.

McDaid AJ and Mace BR (2013) A self-tuning electromagnetic vibration absorber with adaptive shunt electronics. *Smart Materials and Structures* 22: 105013.

Nakamura Y, Fukukita A, Tamura K, et al. (2014) Seismic response control using electromagnetic inertial mass dampers. *Earthquake Engineering & Structural Dynamics* 43: 507–527.

Niederberger D, Behrens S, Fleming AJ, et al. (2006) Adaptive electromagnetic shunt damping. *Proceedings of the IEEE/ASME transactions on mechatronics 2006* 11(1): 103–108.

Palomera-Arias R, Connor JJ and Ochsendorf J (2008) Feasibility study of passive electromagnetic damping systems. *Journal of Structural Engineering* 134(1): 164–170.

Smith MC (2002) Synthesis of mechanical networks: the inerter. *IEEE Transactions on Automatic Control* 47(10): 1648–1662.

Snowdon JC (1968) *Vibration and shock in damped mechanical systems*. Newyork: John Wiley & Sons.

Sodano HA, Bae J-S, Inman DJ, et al. (2005) Concept and model of eddy current damper for vibration suppression of a beam. *Journal of Sound and Vibration* 288: 1177–1196.

Stabile A, Aglietti G, Richardson G, et al. (2017) Design and verification of a negative resistance electromagnetic shunt damper for spacecraft micro-vibration. *Journal of Sound Vibration* 386: 38–49.

Takeya K, Sasiki E and Kobayashi Y (2016) Design and parametric study on energy harvesting from bridge vibration using tuned dual-mass damper systems. *Journal of Sound and Vibration* 361: 50–65.

Tang X, Liu Y, Cui W, et al. (2016) Analytical solutions to H_2 and H_∞ optimizations of resonant shunted electromagnetic tuned mass damper and vibration energy harvester. *Journal of Vibration and Acoustics* 138: 011018.

Tang X and Zuo L (2011) Enhanced vibration energy harvesting using dual-mass systems. *Journal of Sound and Vibration* 330: 5199–5209.

Thomas O, Deü J-F and Ducarne J (2009) Vibration of an elastic structure with shunted piezoelectric patches: efficient finite-element formulation and electromechanical coupling coefficients. *International Journal of Numerical Methods in Engineering* 80(2): 235–268.

Thomas O, Ducarne J and Deü J-F (2012) Performance of piezoelectric shunts for vibration reduction. *Smart Materials and Structures* 21(1): 015008.

Thomas O, Touzé C and Chaigne A (2003) Asymmetric nonlinear forced vibrations of free-edge circular plates, part 2: experiments. *Journal of Sound and Vibration* 265(5): 1075–1101.

Vakilinejad M, Grolet A and Thomas O (2019) A comparison of robustness and performance of linear and non linear lanchester dampers. *Nonlinear Dynamics* 100: 269–287.

Yan B, Wang K, Hu Z, et al. (2017) Shunt damping vibration control technology: a review. *Applied Sciences* 7, 494.

Yan B, Zhang X, Luo Y, et al. (2014) Negative impedance shunted electromagnetic absorber for broadband absorbing: experimental investigation. *Smart Materials anf Structures* 23, 125044.

Zhou S, Jean-Mistral C and Chesné S (2019) Electromagnetic shunt damping with negative impedances: optimization and analysis. *Journal of Sound and Vibration* 445: 188–203.

Zhu S, Shen W-A and Xu Y-L (2012) Linear electromagnetic devices for vibration damping and energy harvesting: modeling and testing. *Engineering Structures* 34: 198–212.

Zhu S, Shen W and Qian X (2013) Dynamic analogy between an electromagnetic shunt damper and a tuned mass damper. *Smart Materials and Structures* 22: 115018.

Zuo L, Chen X and Nayfeh S (2011) Design and analysis of a new type of electromagnetic damper with increased energy density. *Journal of Vibration and Acoustics* 133: 041006.

Zuo L and Cui W (2013) Dual-functional energy-harvesting and vibration control : electromagnetic resonant shunt series tuned mass dampers. *Journal of Vibration and Acoustics* 135(5): 051018.

Appendix 1

Fixed points for the simple dampers

To optimise all the dampers, the method used in (Liu and Liu, 2005; Snowdon, 1968) is followed. The frequencies of the fixed points and the corresponding amplitude of $|\hat{x}_1(\Omega)|$ are given by:

- Lanchester damper:

$$\omega_F = \omega_1 \sqrt{\frac{2}{2+\mu}}, \qquad |\hat{x}_1(\omega_F)| = \frac{F_0}{m_1 \omega_1^2} \frac{2+\mu}{\mu} \quad \text{(A.1)}$$

- R-shunt:

$$\omega_F = \omega_1 \sqrt{\frac{2+\kappa^2}{2}}, \qquad |\hat{x}_1(\omega_F)| = \frac{F_0}{m_1 \omega_1^2} \frac{2}{\kappa^2} \quad \text{(A.2)}$$

- DVA:

$$\omega_{F,G} = \omega_1 \sqrt{\frac{1 \pm \sqrt{\mu/(2+\mu)}}{1+\mu}},$$

$$|\hat{x}_1(\omega_F)| = \frac{F_0}{m_1 \omega_1^2} \sqrt{\frac{2+\mu}{\mu}} \quad \text{(A.3)}$$

- RC-shunt:

$$\omega_{F,G} = \omega_1 \sqrt{\frac{2 \pm \sqrt{2}\kappa}{2}}, \qquad |\hat{x}_1(\omega_F)| = \frac{F_0}{m_1 \omega_1^2} \frac{\sqrt{2}}{\kappa} \quad \text{(A.4)}$$

Appendix 2

Optimisation of the CDVA coupled to the R-shunt

We consider the case of architecture 2 with a CDVA and a R-shunt, considered in section 4.2.1. The frequency response of the system is obtained by writing equations (27a,b) and (14a) in the frequency domain:

$$\hat{x}_1 = \frac{F_0}{m_1} \frac{(-\Omega^2 + \lambda_e j\Omega)(-\Omega^2 + \omega_2^2)}{D_{\text{CDVA}-\text{R}}(\Omega)} \quad \text{(B.1)}$$

with

$$D_{\text{CDVA}-\text{R}}(\Omega) = -\Omega^2[\Omega^4 - [(1+\mu)\omega_2^2 + (1+\kappa^2)\omega_1^2] \\ \Omega^2 + (1+\kappa^2)\omega_1^2\omega_2^2] \quad \text{(B.2)}$$

$$+ j\lambda_e\Omega[\Omega^4 - [\omega_1^2 + (1+\mu)\omega_2^2]\Omega^2 + \omega_1^2\omega_2^2]. \quad \text{(B.3)}$$

This can be rewritten:

$$\hat{x}_1 = \frac{F_0}{m_1} \frac{A(\Omega) + j\lambda_e B(\Omega)}{C(\Omega) + j\lambda_e D(\Omega)}. \quad \text{(B.4)}$$

The frequencies of the fixed points F and G of Figure 10, which are common to all the curves obtained by varying λ_e, in particular if $\lambda_e = 0$ and $\lambda_e \to +\infty$, are the Ω solutions of:

$$|\hat{x}_1(\Omega)|_{\lambda_e=0} = |\hat{x}_1(\Omega)|_{\lambda_e=+\infty} \quad \Rightarrow \quad \frac{A}{C} = \pm\frac{B}{D} \quad \text{(B.5)}$$
$$\Rightarrow \quad A(\Omega)D(\Omega) \pm B(\Omega)C(\Omega) = 0.$$

The equation $AD + BC = 0$ has the trivial solutions $\Omega = 0$ and $\Omega = \omega_2$. The equation $AD - BC = 0$ can be written $-\Omega^3(\Omega^2 - \omega_2^2)K(\Omega) = 0$ in which $K(\Omega)$ is a second order polynomial in Ω^2, whose positive roots are given in equation (40). Then, substituting equation (40) in equation (B.1) and simplifiying the result using symbolic computations gives equation (38) for the common amplitude of the fixed points.

Finally, we are interested in the value of λ_e that gives the frequency response with a horizontal tangent at point F (resp. at point G). We write:

$$|\hat{x}_1|^2 = \frac{A^2 + \lambda_e^2 B^2}{C^2 + \lambda_e^2 D^2}, \quad \text{(B.6)}$$

so that $\partial|\hat{x}_1|^2/\partial\Omega(\Omega = \omega_{F,G}) = 0$ is equivalent to

$$(BB'D^2 - DD'B^2)\lambda_e^4 + (BB'C^2 + AA'D^2 - DD'A^2 - CC'B^2) \\ \lambda_e^2 + AA'C^2 - CC'A^2 = 0. \quad \text{(B.7)}$$

This equation can be solved analytically for λ_e, which leads to huge expressions in term of ω_2, κ and μ (ω_1 can be set to one without loss of generality). However, it was numerically verified that $\lambda_e = \omega_{F,G}$ enables to exactly verify equation (B.7), which gives the solution.

Appendix 3

Optimisation details for the CDVA/RC-shunt coupling

The same procedure as in the previous section is applied to the CDVA/RC-shunt case, with λ_e replaced by ξ_e in equations (B.4), (B.6) and (B.7). The method initiated in (Brock, 1946) and successfully used in (Liu and Liu, 2005; Snowdon, 1968) for the simple absorbers was tested and gave no better results here, since the orders of $A(\Omega)$, $B(\Omega)$, $C(\Omega)$ and $D(\Omega)$ in Ω are higher.